Reviewed Preprint
v1 • September 5, 2025
Not revised

Reviewed Preprint
v2 • February 23, 2026
Revised by authors

Mycobacterial Metallophosphatase MmpE acts as a Nucleomodulin to Regulate Host Gene Expression and Promote Intracellular Survival

Liu Chen[1,2], Baojie Duan[1], Qiang Jiang[1], Yifan Wang[1], Yingyu Chen[1,3], Lei Zhang[1,3] ✉, Aizhen Guo[1,2,3] ✉

[1]National Key Laboratory of Agricultural Microbiology, College of Veterinary Medicine, Huazhong Agricultural University, Wuhan, China • [2]Hubei Hongshan Laboratory, Huazhong Agricultural University, Wuhan, China • [3]National Professional Laboratory for Animal Tuberculosis, Ministry of Agriculture and Rural Affairs, Huazhong Agricultural University, Wuhan, China

For correspondence:
zhanglei2023@mail.hzau.edu.cn
aizhen@mail.hzau.edu.cn

Competing interests: No competing interests declared

Funding: See page 31

Reviewing editor: Amit Singh, Indian Institute of Science, India

eLife Assessment

The work **convincingly** demonstrates the role of the mycobacterial secreted effector protein MmpE, which translocates to the host nucleus and exhibits phosphatase activity. The study is particularly **valuable** in showing that both the nuclear localization signal sequences and residues critical for phosphatase function are essential for host gene regulation, lysosomal biogenesis, and intracellular survival. Future studies will be needed to explore additional host pathways modulated by MmpE, particularly in the context of infection with a fully virulent Mycobacterium tuberculosis strain.

https://doi.org/10.7554/eLife.108037.2.sa4

Abstract

Mycobacterium tuberculosis, the causative agent of tuberculosis, remains a major global health challenge. Nucleomodulins, bacterial effectors that target the host cell nuclei, are increasingly recognized as key virulence factors, but their roles in mycobacterial pathogenesis remain incompletely elucidated. Here, we characterize a hypothetical protein Rv2577 (designated MmpE) not only as a Fe^{3+}/Zn^{2+}-dependent metallophosphatase but also as a critical nucleomodulin involved in immune evasion and intracellular persistence. MmpE utilizes two nuclear localization signals, $RRR^{20\text{-}22}$ and $RRK^{460\text{-}462}$, to enter the host cell nucleus, where it binds to the promoter region of the vitamin D receptor (VDR) gene, thereby inhibiting host inflammatory gene expression. Additionally, MmpE regulates the PI3K-Akt-mTOR signaling pathway, thereby arresting lysosome maturation. These actions collectively facilitate immune suppression and promote mycobacterial survival in macrophages and in mice. Our findings identify MmpE as a conserved nucleomodulin in mycobacteria and reveal a novel mechanism of MmpE-mediated intracellular survival.

Introduction

Mycobacterium tuberculosis (Mtb), the etiological agent of tuberculosis, has posed a persistent global health burden for centuries. Despite significant advances in elucidating the molecular mechanisms of its pathogenesis, current research has largely focused on effector proteins that modulate host cell membrane and cytoplasmic processes (Nisa et al., 2022; Nasiri and Venketaraman, 2025). In contrast, investigations into effector proteins that target the host cell nucleus, the central hub for gene regulation and cellular control, remain comparatively limited.

Nucleomodulins are a class of bacterial effector proteins that can translocate into the host nucleus, where they modulate nuclear processes to promote pathogen survival (Chai et al., 2020; Bierne and Cossart, 2021). These proteins affect host gene expression by directly interacting with chromatin or by mimicking transcription factors, chromatin modifiers, or other nuclear regulators (Li et al., 2013; Rolando et al., 2013; Mitra et al., 2018; Hanford et al., 2021). For instance, LntA from *Listeria monocytogenes* directly binds the chromatin repressor BAHD1, disrupting its function and derepressing interferon-stimulated genes in a type III interferon-dependent manner, ultimately promoting bacterial persistence (Lebreton et al., 2011; Lebreton et al., 2014). Similarly, Ank1 and Ank6 from *Orientia tsutsugamushi* localize to the host nucleus and facilitate the export of the NF-κB p65 subunit via exportin 1, thereby suppressing the transcription of pro-inflammatory genes (Evans et al., 2018; Steiert and Weber, 2025). Although bacterial nucleomodulins utilize diverse strategies to manipulate host nuclear functions, the identity and functional characterization of *M. tuberculosis* nucleomodulins remain poorly defined.

Nucleomodulins employ various strategies to enter access to the host cell nucleus, including passive diffusion, hijacking host proteins that contain nuclear localization signals (NLSs), or using of their own NLSs to interact with the nuclear pore complex (Hanford et al., 2021). Among these mechanisms, NLSs play a particularly important role. Classical NLSs are further divided into monopartite (MP) and bipartite (BP) forms. Monopartite NLSs consist of a single cluster of 4-8 basic residues, primarily lysine (K) or arginine (R), with a typical consensus motif of K-K/R-X-K/R (Fontes et al., 2000; Kosugi et al., 2009; Cautain et al., 2015). Nuclear localization enables these effectors to manipulate host gene expression, disrupt immune signaling, and reprogram cellular processes to promote pathogen survival. For example, EspF from enteropathogenic *Escherichia coli* contains an N-terminal NLS that directs it to the nucleolus, where it interferes with ribosome biogenesis (Dean et al., 2010; Singh et al., 2018). NUE, a SET domain-containing nucleomodulin secreted by *Chlamydia trachomatis*, also possesses an NLS that mediates its nuclear localization, where it functions as a histone lysine methyltransferase (HKMTase) targeting host histones H2B, H3, and H4 (Pennini et al., 2010; Jermy, 2010).

Beyond their nuclear localization capabilities, some nucleomodulins directly affect host immunity through intrinsic enzymatic activities Agarwal et al., 2012). For example, the nucleomodulin PtpA promotes Mtb survival within macrophages by dephosphorylating host cytoplasmic proteins (Wang et al., 2017). NleC from *E. coli*, a Zn^{2+}-dependent metalloprotease, suppresses host immune responses by cleaving the p65 subunit of NF-κB in the cytoplasm, thereby inhibiting its nuclear translocation, and can enter the nucleus to reduce nuclear p65 levels, blocking NF-κB-dependent transcription of pro-inflammatory genes (Baruch et al., 2011; Hodgson et al., 2015). Among these enzymatically active nucleomodulins, purple acid phosphatases (PAPs) represent a distinct and functionally significant, yet underexplored, subclass within the metallophosphatase superfamily. PAPs are characterized by a conserved β-α-β-α-β fold and five signature motifs (DxG, GDXXY, GNH[D/E], VXXH, GHXH), which coordinate seven metal-ligating residues at a binuclear metal center (Rodriguez et al., 2014; Bhadouria et al., 2017; Bhadouria and Giri, 2022). These enzymes have been extensively studied in plants and mammals, where they are involved in key biological processes such as phosphorus metabolism and the generation of reactive oxygen species (Comba et al., 2013; Feder et al., 2020; Liu et al., 2025). However, only a few bacterial PAPs have been identified, such as BcPAP from *Burkholderia cenocepacia*, and their functions remain largely unknown (Yeung et al., 2009). Notably, in Mtb, MmpE is the only identified PAP protein (Schenk et al., 2000), but its specific contribution to infection and pathogenesis remain elusive.

In this study, we characterized MmpE as a conserved nucleomodulin in mycobacteria and demonstrated its nuclear translocation mediated by two functional motifs. Nuclear-localized MmpE regulates host immune responses by repressing the vitamin D receptor (VDR), a key regulator of antimicrobial gene expression, and disrupting lysosome maturation through suppression of the PI3K-Akt-mTOR signaling pathway. Additionally, MmpE exhibits Fe^{3+}-dependent

metallophosphatase activity, contributing to intracellular survival. These findings establish MmpE as a bifunctional effector that integrates immune modulation and enzymatic catalysis, underscoring its role in mycobacterial pathogenesis and potential as a therapeutic target.

Results

NLSs are required for the nuclear translocation of MmpE

In a prior study, we screened conserved nucleomodulins in Mtb and found that hypothetical protein Rv2577 (MmpE) exhibits strong nuclear localization in HEK293T cells (Chen et al., 2025). Furthermore, we observed a time-dependent increase in nuclear MmpE-EGFP levels in HEK293T cells (Figure 1A, Figure S1A). Nuclear-cytoplasmic fractionation assays further confirmed these results, showing a progressive enrichment of MmpE in the nucleus during the course of transfection (Figure 1B), suggesting that MmpE might possess a nuclear translocation ability.

MmpE contains two putative nucleus localization signals, NLS1 (RRR^{20-22}) and NLS2 ($RRK^{460-462}$) which are located in the loop regions of the MmpE structure predicted by AlphaFold (Figure 1C). Deleting either the individual NLSs or both simultaneously does not lead to a conformational change in the core structure (Figure S1B). To assess the effects of NLSs on nuclear localization, we constructed NLS-deleted mutants, including $MmpE^{\Delta NLS1}$, $MmpE^{\Delta NLS2}$, and $MmpE^{\Delta NLS1-2}$ and transfected them into HEK293T cells. Fluorescence microscopy at 36 hours post-transfection (hpt) revealed that deletion of either NLS significantly reduced nuclear accumulation of MmpE-EGFP, while simultaneous deletion of both NLS motifs ($MmpE^{\Delta NLS1-2}$) completely abolished nuclear localization, resulting in exclusive cytoplasmic distribution (Figure 1D and E). Consistent with the microscopy results, nuclear-cytoplasmic fractionation showed that WT MmpE was present in detected both cytoplasmic and nuclear fractions, whereas $MmpE^{\Delta NLS1}$ and $MmpE^{\Delta NLS2}$ exhibited substantially reduced nuclear levels. Notably, the double mutant $MmpE^{\Delta NLS1-2}$ was completely undetectable in the nucleus (Figure 1F and G), suggesting that both NLS motifs are necessary for nuclear import.

To further detect whether MmpE translocates into the host nucleus during mycobacterial infection, we conducted recombinant *M. bovis* BCG strains expressing C-terminally Flag-tagged WT MmpE or the NLS deletion mutants including $MmpE^{\Delta NLS1}$, $MmpE^{\Delta NLS2}$ and $MmpE^{\Delta NLS1-2}$. Immunoblot analysis of culture filtrates showed that both MmpE-Flag and the secreted antigen Ag85B were detectable in the supernatant of wild-type strains, whereas secretion of $MmpE^{\Delta NLS1}$ or $MmpE^{\Delta NLS1-2}$ was barely detectable. These observations indicate that MmpE is secreted by BCG and that NLS1 is essential for its efficient export (Figure S1C). Following infection of THP-1 macrophages, nuclear-cytoplasmic fractionation revealed that wild-type MmpE localized to both cytoplasmic and nuclear compartments, while $MmpE^{\Delta NLS1}$, $MmpE^{\Delta NLS2}$or $MmpE^{\Delta NLS1-2}$ were almost undetectable in nuclear fractions (Figure S1D). These findings indicate that nuclear localization of MmpE depends on two distinct NLS motifs, with NLS2 being essential for effective nuclear translocation.

Deletion of NLSs does not alter the phosphatase activity of MmpE

MmpE is a putative a Fe^{3+}/Zn^{2+}-metallophosphatase with a purple acid phosphatase (PAP) motif (Figure 2A; Figure S2A). Multiple sequence alignment and phylogenetic reconstruction revealed that MmpE is highly conserved across mycobacterial species and harbors canonical characteristics of metallophosphatases with GD, GNHX, and GHXH motifs (Figure 2B, Figure S2B). These motifs are typically associated with enzymes that catalyze phosphate hydrolysis via a binuclear metal ion-dependent mechanism, wherein residues such as Asp, His, and Asn coordinate essential metal cofactors, commonly Fe^{3+}, Mn^{2+}, or Zn^{2+}, at the active site. To test this, recombinant MBP-tagged MmpE without the Tat signal peptide ($MmpE^{\Delta Tat}$) was purified and subjected to *in vitro* phosphatase assays using *p*-nitrophenyl phosphate (*p*-NPP) as the substrate. Different concentrations of Fe^{3+} or Zn^{2+} were added to the reactions to detect their effects on the enzyme activity of MmpE. At the same ion concentrations, Fe^{3+} is more effective than Zn^{2+} in stimulating MmpE hydrolysis of *p*-NPP. The maximal enzymatic activity was observed at 50 μM

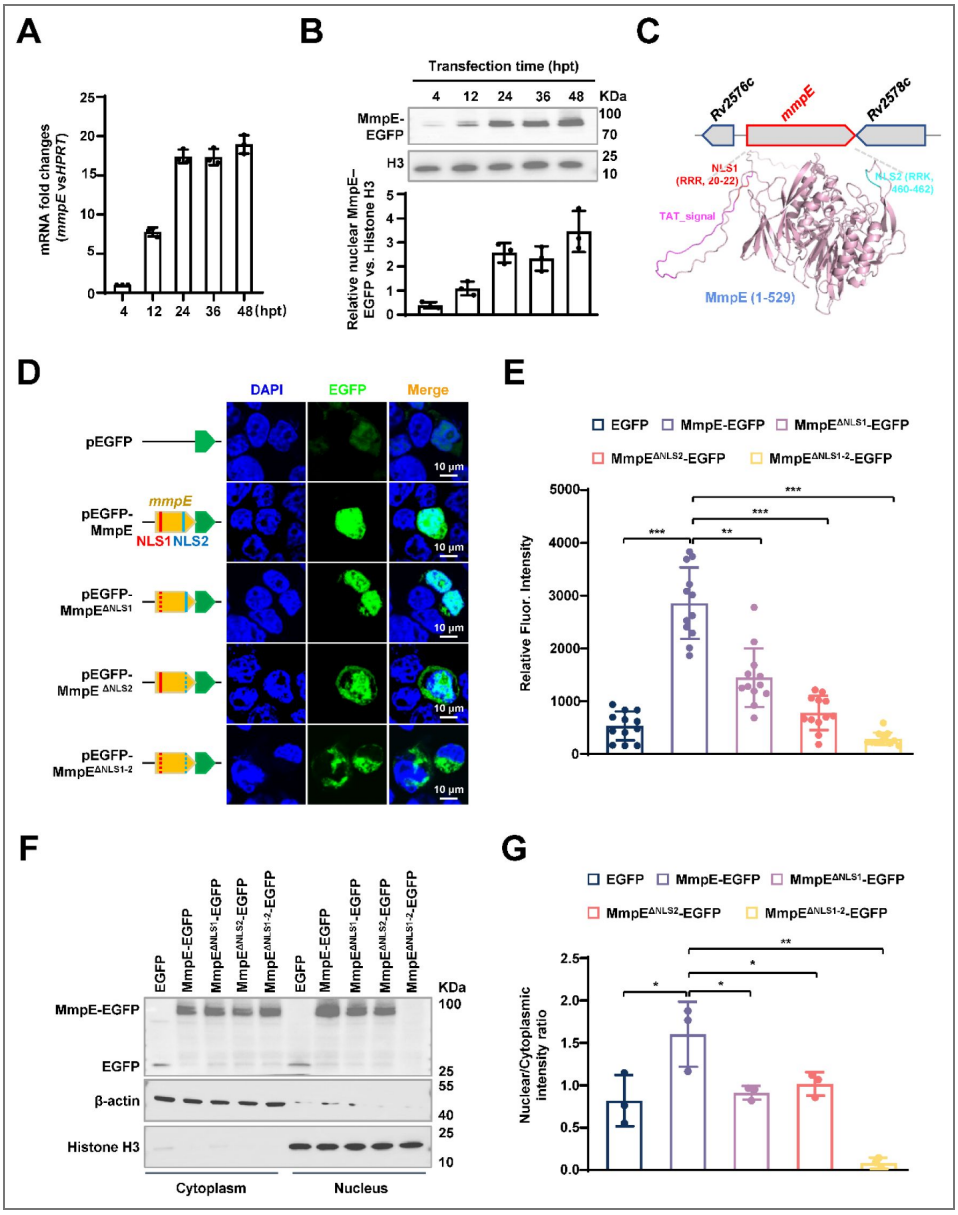

Figure 1. NLSs are required for the nuclear translocation of MmpE.

(A) qRT-PCR analysis of *mmpE* mRNA expression in HEK293T cells over 48 hpt. **(B)** Western blot analysis of nuclear fractions showing time-dependent accumulation of MmpE-EGFP (top), and corresponding quantification of nuclear MmpE-EGFP levels (bottom). Histone H3 and β-actin were used as nuclear and cytoplasmic markers, respectively. **(C)** Domain architecture of MmpE, including a Tat signal peptide (1-54 amino acids, with a twin-arginine translocation motif) and two nuclear localization signals (NLS1: 20-22 aa; NLS2: 460-462 aa). The structure of the MmpE protein was predicted using AlphaFold 2.2.0, with NLS1 and NLS2 highlighted in red and green, respectively. **(D)** Subcellular localization of EGFP-tagged wild-type and NLS-deleted MmpE. (left) Schematic representation of EGFP-tagged constructs. (right) Confocal microscopy images of HEK293T cells transfected with the indicated constructs for 36 hpt. EGFP fluorescence (green) and nuclear staining with DAPI (blue) were visualized using an FLUOVIEW software (v5.0). Scale bar, 10 μm. Images were acquired with a ×100 oil immersion objective (NA = 1.4). **(E)** Quantification of nuclear EGFP intensity of wild-type and mutant MmpE in (Figure 1D). Data are shown as mean ± SD, n = 12 cells. **(F)** Western blot analysis of nuclear and cytoplasmic fractions from HEK293T cells transfected with wild-type and mutant MmpE-EGFP confirmed their subcellular localization. MmpE-EGFP was detected using an anti-GFP antibody, and histone H3 and β-actin served as nuclear and cytoplasmic markers, respectively. **(G)** Quantitative analysis of MmpE-EGFP levels in the cytoplasmic and nuclear compartments of (Figure 1F). Data represent mean ± SD of three independent biological replicates. Statistical significance determined using two-tailed unpaired Student's *t*-tests, $*P < 0.05$, $**P < 0.01$, $***P < 0.001$.

Fe^{3+} (Figure 2C). To identify the key residues of MmpE involved in metal coordination, molecular docking experiment was performed using PyMOL on the structure of MmpE predicted by AlphaFold. His348 and Asn359 are supposed to be involved in metal ion coordination within the active site (Figure 2D). Then, the double mutant $MmpE^{\Delta Tat}$-H348A/N359A was conducted to verify the essential residues for enzyme activity. As shown in Figure 2E, the addition of 50 μM Fe^{3+} significantly increased the *in vitro* phosphatase activity of $MmpE^{\Delta Tat}$ compared to reactions without metal ions. However, the enzymatic activity of the $MmpE^{\Delta Tat}$-H348A/N359A was significantly reduced under the same conditions, indicating that the residues His348 and ASN359 are essential for metal binding and catalytic activity. Additionally, we found that deletion of the NLSs does not affect the phosphatase activity of MmpE (Figure 2F), consistent with the observation on comparison of the structures (Figure S1B). Collectively, these results indicates that MmpE is a highly conserved Fe^{3+}-dependent metallophosphatase in mycobacteria, and its enzymatic activity is independent of the NLSs.

The nuclear translocation and phosphatase activity of MmpE are essential for *M. bovis* BCG survival in macrophage cells

To examine whether MmpE is important for bacterial intracellular survival, we constructed *mmpE*-deletion mutant (ΔMmpE) in BCG strain by homologous recombination (Figure S3A-C). The ΔMmpE mutant and the ΔMmpE strains complemented with WT *mmpE* (Comp-MmpE) or NLS-deleted *mmpE* (Comp-$MmpE^{\Delta NLS1}$, Comp-$MmpE^{\Delta NLS2}$, and Comp-$MmpE^{\Delta NLS1\text{-}2}$) exhibited similar growth rate in the standard 7H9 media (Figure S3D). During infection of THP-1 macrophages, the ΔMmpE strain exhibited a significantly reduced intracellular bacterial burden and accelerated clearance compared to the WT strain, while this phenotype was restored by complementation with wild-type MmpE. Importantly, the load of the Comp-$MmpE^{\Delta NLS2}$ displayed significantly lower compared to Comp-MmpE in THP-1 cells (Figure 3A). A comparable phenotype was also observed in RAW264.7 macrophages (Figure 3B). These findings indicate that NLS2-mediated nuclear localization is critical for the intracellular function of MmpE. Furthermore, the Comp-$MmpE^{\Delta NLS1}$ and Comp-$MmpE^{\Delta NLS1\text{-}2}$ strains showed partial restoration of bacterial load compared to the ΔMmpE strain, but remained lower than those of the Comp-MmpE strain (Figure 3C and D). These results demonstrate that both NLSs are critical for MmpE-mediated bacterial survival within macrophages. Given that MmpE functions as a Fe^{3+}-dependent metallophosphatase in mycobacteria, we examined whether its enzymatic activity contributes to intracellular persistence and constructed a phosphatase-deficient double mutant strain (Comp-MmpE-H348A/N359A) (Figure S3E) to infect THP-1 macrophage. The result showed that a significantly reduced intracellular bacterial burden compared to Comp-MmpE, indicating that the phosphatase activity also plays an important role in MmpE-mediated bacterial survival (Figure 3E). To further investigate the underlying mechanism, we analyzed cytokine expression in infected macrophages. Cells infected with the ΔMmpE and Comp-$MmpE^{\Delta NLS1\text{-}2}$ strains exhibited significantly increased levels of pro-inflammatory cytokine, including *IL1A*, *IL1B*, and *IL6*, compared to the WT and Comp-MmpE strains. Furthermore, in comparison to the Comp-MmpE strains, cells infected with the Comp-$MmpE^{\Delta NLS1}$, Comp-$MmpE^{\Delta NLS2}$, and Comp-MmpEH348A/N359A strains also demonstrated substantial upregulation of these cytokines (Figure 3F-H). Collectively, these results suggest that both nuclear localization and phosphatase activity are essential for the immunomodulatory function of MmpE, which facilitates bacterial survival by suppressing host inflammatory responses.

MmpE regulates host transcription network involved in inflammation response and lysosomal maturation

To investigated the effect of MmpE on host gene expression, we performed RNA-seq experiments on THP-1 macrophages infected with WT or ΔMmpE at 24 hpi. A total of 175 differentially expressed genes (DEGs) were identified, with 142 upregulated and 33 downregulated in ΔMmpE-infected cells compared to WT-infected cells (Figure 4A, Table S2). Gene ontology (GO) analysis revealed significant enrichment in immune-related biological processes, including

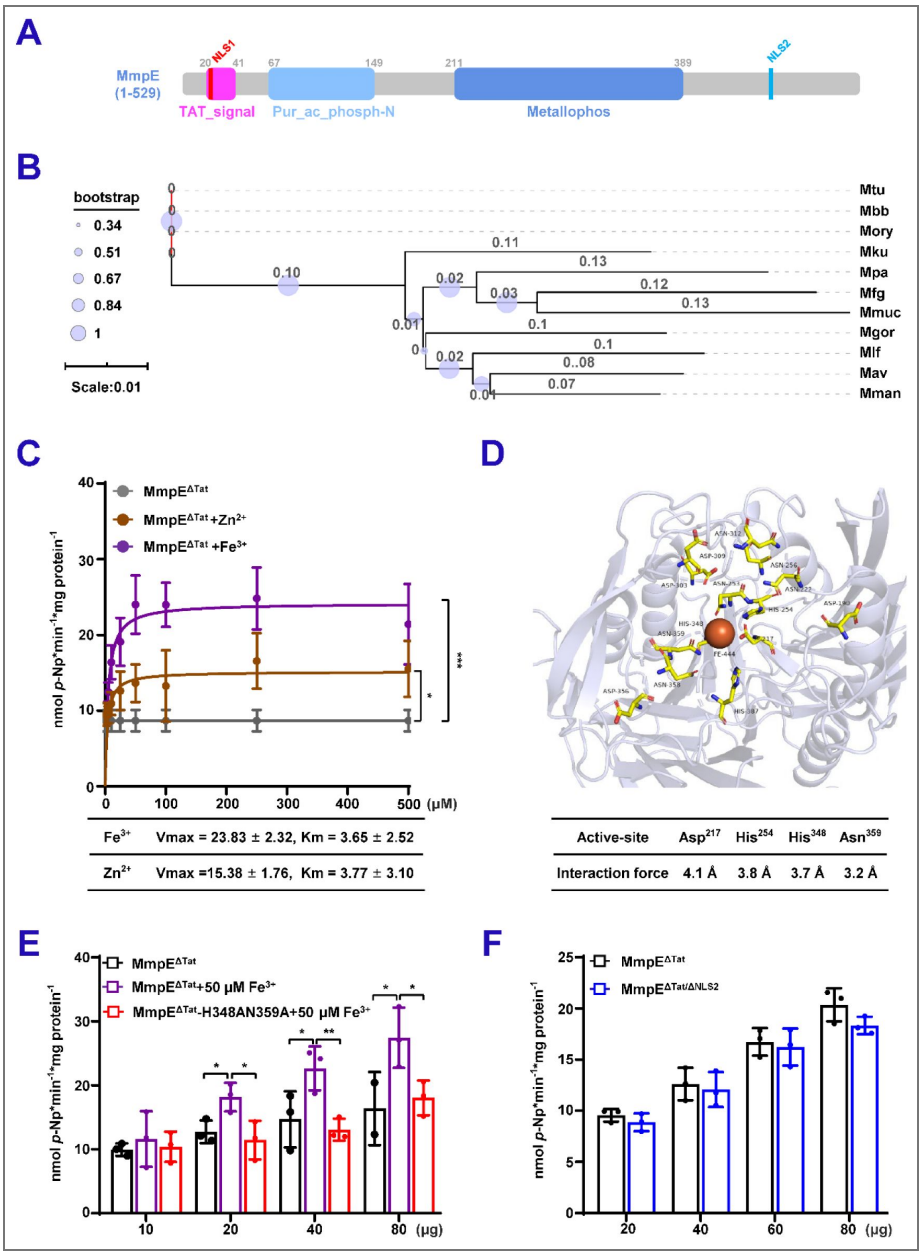

Figure 2. Deletion of NLSs does not alter the phosphatase activity of MmpE.

(**A**) Domain architecture of MmpE. Schematic representation of MmpE with the annotated functional domains, including a Tat signal peptide (1-41 aa, twin-arginine translocation motif), a purple acid phosphatase domain (68-149 aa), a calcineurin-like phosphoesterase domain (211-389 aa) and two nuclear localization signals (NLS1: 20-22 aa; NLS2: 460-462 aa). (**B**) Phylogenetic and structural conservation of MmpE. Neighbor-joining phylogenetic tree of MmpE homologs across Mycobacterium species (1,000 bootstrap replicates; values ≥50% shown). Species abbreviations: *M. tuberculosis* (Mtu), *M. bovis* BCG (Mbb), *M. orygis* (Mory), *M. kubicae* (Mku), *M. paraterrae* (Mpa), *M. farcinogenes* (Mfg), *M. mucogenicum* (Mmuc), *M. vicinigordonae* (Mgor), *M. lentiflavum* (Mlf), *M. avium* (Mav), *M. manitobense* (Mman). **(C)** Phosphatase activity of MmpE$^{\Delta Tat}$ (lacking the N-terminal Tat signal peptide) was measured using *p*-NPP as the substrate in the presence of increasing concentrations (0-500 μM) of Fe^{3+} and Zn^{2+}. **(D)** Prediction of metal ion-binding residues in MmpE. Structural modeling and visualization were performed using PyMOL. Conserved residues in the putative metal-binding pocket are shown as sticks, colored by atom type. The predicted metal coordination site is highlighted, with key binding residues labeled. Surface representation depicts the spatial accessibility of the pocket. (**E**) Phosphatase activity of increasing concentrations of MmpE$^{\Delta Tat}$ and the mutant MmpE$^{\Delta Tat}$-H348AN359A was measured in the absence or presence of 50 μM Fe^{3+}. (**F**) Phosphatase activity of increasing concentrations of MmpE$^{\Delta Tat}$ and MmpE$^{\Delta Tat/\Delta NLS1\text{-}2}$ was measured under standard conditions. Data represent mean ± SD of three independent biological replicates. Statistical significance determined using two-way ANOVA, $*P < 0.05$, $**P < 0.01$, $***P < 0.001$.

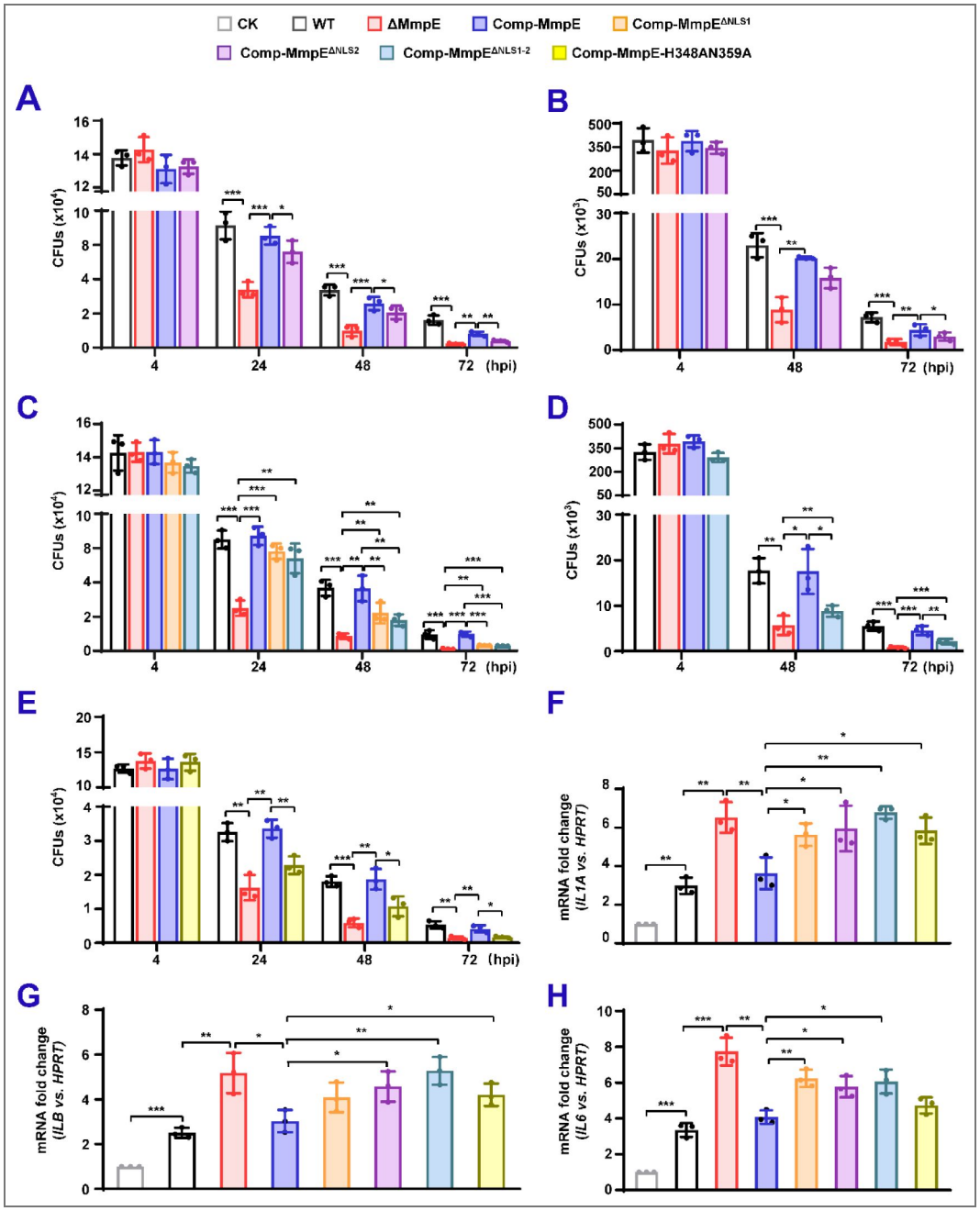

Figure 3. The nuclear translocation and phosphatase activity of MmpE are essential for *M. bovis* BCG survival in macrophage cells.

(A-B) Intracellular survival of BCG strains in human THP-1 macrophages **(A)** and RAW264.7 macrophages (**B**). Strains include BCG WT, ΔMmpE, Comp-MmpE, and Comp-MmpE$^{\Delta NLS2}$. **(C-D)** Intracellular survival of strains in THP-1 (**C**) and RAW264.7 macrophages (**D**). Strains include BCG WT, ΔMmpE, Comp-MmpE, Comp-MmpE$^{\Delta NLS1}$and Comp-MmpE$^{\Delta NLS1-2}$. **(E)** Intracellular survival of Comp-MmpE-H348AN359H mutant in THP-1 cells. **(F-H)** Inflammatory cytokine expression in infected THP-1 cells. mRNA levels of *IL-1A* (**F**), *IL-1B* (**G**), and *IL-6* (**H**) were quantified by qRT-PCR 24 hpi with the indicated BCG strains. Data represent mean ± SD of three independent biological replicates. Statistical significance determined using two-way ANOVA or two-tailed unpaired Student's *t*-tests, **P* < 0.05, ***P* < 0.01, ****P* < 0.001.

apoptosis and cell death, molecular functions associated with immune activation and cellular stress responses such as pyrophosphatase activity and nucleoside-triphosphatase activity (Figure 4B). KEGG pathway enrichment analysis showed that these DEGs were primarily involved in immune and inflammatory signaling pathways, including cytokine-cytokine receptor interaction, TNF, Toll-like receptor, chemokine, NF-κB, JAK-STAT, and PI3K-Akt signaling pathways. Additionally, a subset of DEGs was involved in lysosome-associated host pathways, consistent with previous findings that MmpE inhibits lysosomal maturation (Forrellad et al., 2020) (Figure 4C). To further explore the functional relevance of the DEGs, we performed protein-protein interaction (PPI) network analysis focusing on protein-coding genes, which accounted for 38% of the total DEGs (Figure S4C). The results suggested that some core proteins including IL23A, IL12B, CSF2, CD69, IDO1, and CEACAM1, are mainly related to the production of inflammatory cytokine and immune regulation (Figure 4D). Consistently, these genes showed increased expression in ΔMmpE-infected macrophages compared to those infected with wild-type BCG (Figure 4E). These results suggest that MmpE suppresses immune and lysosome-associated gene expression during infection.

Further, we performed qRT-PCR to confirm the expression of key lysosomal maturation markers, including *TFEB*, *LAMP1*, *LAMP2*, and several V-ATPase subunit genes (*ATP6V0A1*, *ATP6V0C*, *ATP6V1A*, *ATP6V1B2*, and *ATP6V1E1*), as well as inflammatory cytokine. The expression levels of these genes were significantly higher in ΔMmpE-infected macrophages compared to those infected with WT (Figure 4F and G). Moreover, infection with the Comp-MmpE$^{\Delta NLS1-2}$ strain resulted in significantly increased gene expression compared to the Comp-MmpE strain (Figure S4B-D). Taken together, these results suggest that MmpE suppresses host immune and lysosomal responses to facilitate immune evasion during infection.

MmpE regulates the PI3K-Akt-mTOR signaling pathway during macrophage infection

Given that MmpE modulates host transcriptional responses and functions as a nucleomodulin, we investigated whether it associates with host chromatin to regulate gene expression. Cleavage under targets and tagmentation (CUT&Tag) was performed in HEK293T cells transfected with MmpE-EGFP. A total of 2,903 putative MmpE-binding sites were identified (Table S3), of which 18.49% (n = 537) were located in intergenic regions and 39.44% (n = 1,145) in intragenic regions (Figure 5A). Chromosomal mapping revealed preferential enrichment on chromosomes 1 and 2 (Figure 5B). Notably, 99.7% (n = 2,894) of these binding sites were associated with protein-coding genes, and 1,013 of them were located within 3 kb upstream of transcription start sites (TSSs), including 63.18% within 1 kb, 22.9% between 1-2 kb, and 13.92% between 2-3 kb (Figure 5C and D), suggesting that MmpE primarily targets promoter regions to modulate transcription. PPI analysis of the 1,013 putative target genes revealed significant enrichment in immune-related kinases genes, including *PRKCB*, *PLCG2* and *PIK3CB*, which are key regulators of inflammatory signaling and blockes lysosomal maturation via the PI3K-AKT-mTOR pathway (Tian *et al.*, 2020; Zheng et al., 2025) (Figure S5A and B). These findings are consistent with transcriptomic analysis (Figure 4C) and support the hypothesis that MmpE modulates host immune responses, potentially through the PI3K-AKT signaling axis. To validate this hypothesis, we examined activation of the PI3K-AKT-mTOR pathway in THP-1 macrophages infected with either WT or ΔMmpE strains. Immunoblot analysis demonstrated a time-dependent increase in the phosphorylation of AKT (Ser473), mTOR (Ser2448), and p70S6K (Thr389) following WT infection, whereas phosphorylation of these targets was attenuated in cells infected with the ΔMmpE mutant (Figure S5C). To investigate the roles of nuclear localization and phosphatase activity in MmpE-mediated signaling, THP-1 macrophages were infected with WT, ΔMmpE, Comp-MmpE, Comp-MmpE$^{\Delta NLS1}$, Comp-MmpE$^{\Delta NLS2}$, Comp-MmpE$^{\Delta NLS1-2}$, or Comp-MmpE-H348A/N359A. Cells infected with WT or Comp-MmpE exhibited increased phosphorylation of Akt, mTOR, and p70S6K compared to those infected with ΔMmpE and Comp-MmpE$^{\Delta NLS1-2}$ (Figure 5E and F). These results further indicate that nuclear localization is the key determinant of MmpE-mediated activation of the PI3K-AKT-mTOR pathway during mycobacterial infection.

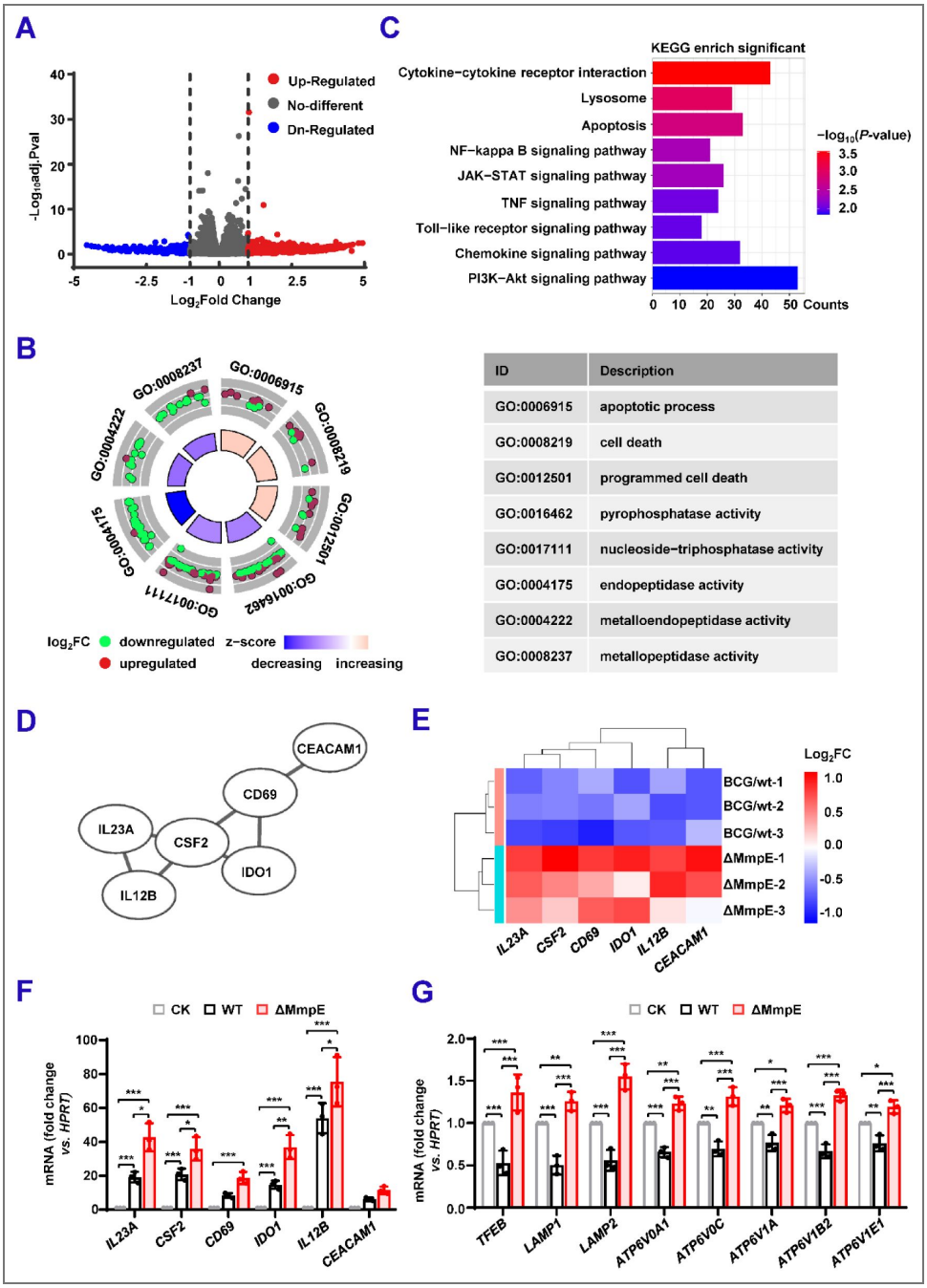

Figure 4. MmpE regulates host transcription network involved in inflammation response and lysosomal maturation.

(A) Volcano plot showing DEGs in THP-1 cells infected with ΔMmpE versus WT strains. DEGs were defined as $|\log_2(\text{fold change})| \geq 1$ and $P < 0.05$. **(B)** Enrichment analysis of DEGs shown in **(A)**. The circular plot shows enriched biological process and molecular function terms. Outer rings represent GO terms (red) and downregulated (green) genes; inner rings reflect z-scores (blue to pink). Selected terms are listed with GO IDs and descriptions. **(C)** KEGG enrichment analysis of DEGs shown in **(A)**. Bar length denotes the number of associated DEGs, and color represents statistical significance ($-\log_{10}$ (*P*-value)). **(D)** Protein-protein interaction network of immune-related DEGs, constructed using STRING v12.0 and visualized in Cytoscape. **(E)** Heatmap of immune-related DEGs in ΔMmpE-infected and WT-infected THP-1 cells. Log_2(fold change) values are shown across three biological replicates. Red and blue indicate upregulation and downregulation, respectively. **(F-G)** qRT-PCR validation of representative DEGs in THP-1 cells infected with WT or ΔMmpE for 24 hpi. Cytokine-related genes (**F**); lysosomal acidification and V-ATPase subunits genes (**G**). Data represent mean ± SD of three independent biological replicates. Statistical significance determined using two-way ANOVA, $^*P < 0.05$, $^{**}P < 0.01$, $^{***}P < 0.001$.

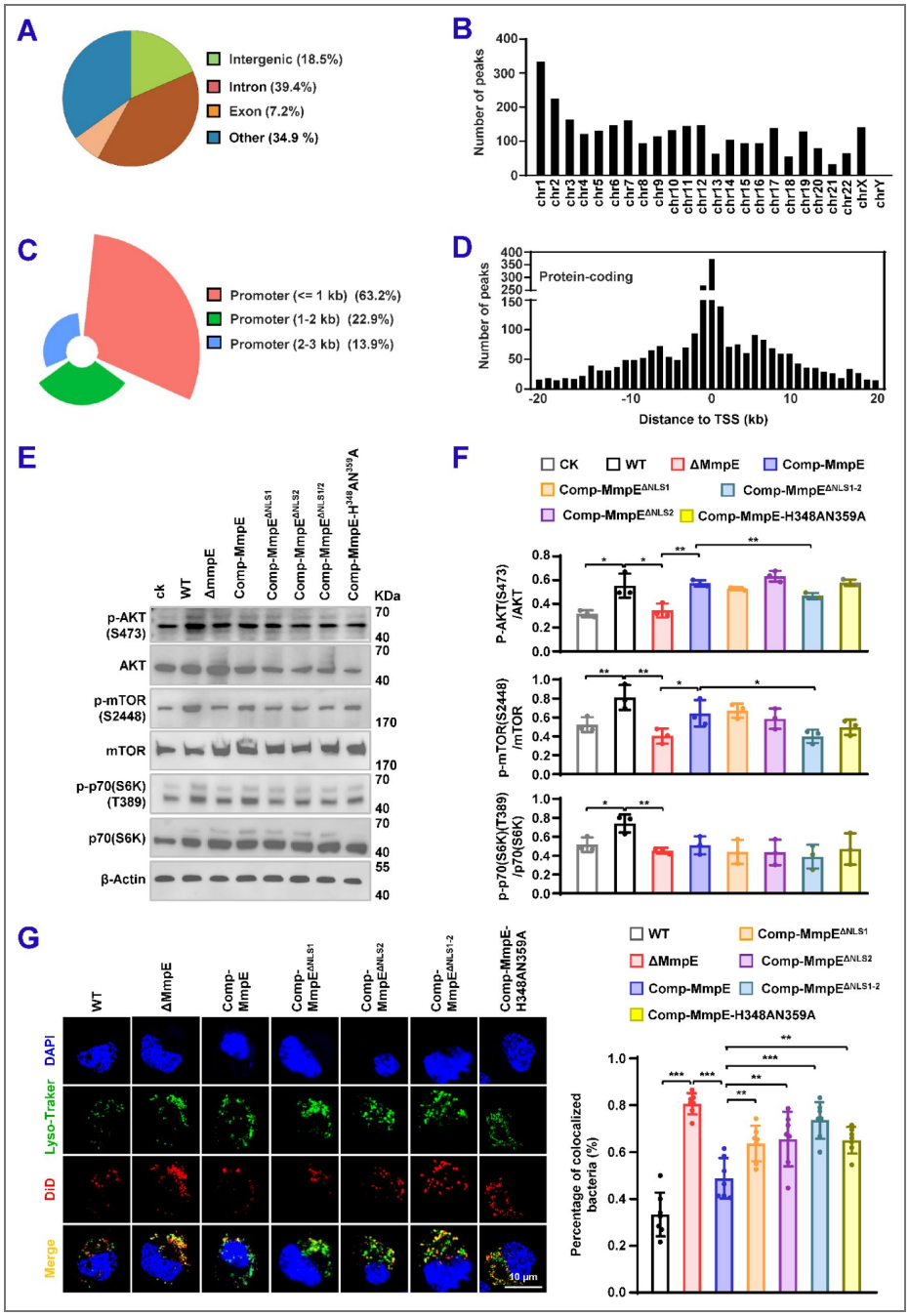

Figure 5. MmpE regulates the PI3K-Akt-mTOR signaling pathway during macrophage infection.

(A-D) Cut&Tag analysis of MmpE-binding regions in HEK293T cells. **(A)** Genomic distribution of potential MmpE-binding regions in HEK293T cells. **(B)** Chromosomal localization of MmpE-enriched peaks (fold enrichment > 9). **(C)** Biotype distribution of potential MmpE-binding regions in HEK293T cells. **(D)** Distribution of binding sites relative to the nearest transcription start sites (TSS) within ±20 kb of protein-coding genes. (**E**) Immunoblot analysis of pathway activation in THP-1 macrophages infected with WT, ΔMmpE, Comp-MmpE, Comp-MmpE$^{\Delta NLS1}$, Comp-MmpE$^{\Delta NLS2}$, Comp-MmpE$^{\Delta NLS1-2}$, or Comp-MmpE-H348A/N359A. Phosphorylation of Akt, mTOR, and p70S6K was evaluated at 8 hpi. **(F)** Quantification of phosphorylation levels across time points. **(G)** (left) Confocal microscopy analysis of phagosome acidification in infected THP-1 macrophages at 24 hpi. Cells were stained with LysoTracker Red and BCG strains were stained with DiD. (right) Co-localization between mycobacteria and LysoTracker was assessed. Representative images showing co-localization of intracellular bacterial with LysoTracker signal. Scale bar, 10 μm. Data represent mean ± SD of three independent biological replicates. Statistical significance determined using two-way ANOVA or two-tailed unpaired Student's *t*-tests, **P* < 0.05, ***P* < 0.01, ****P* < 0.001.

As PI3K-Akt-mTOR signaling is known to inhibits phagolysosomal fusion (Yang et al., 2020), and MmpE downregulates lysosomal genes (Figure 4G), we hypothesized that MmpE may impair lysosomal maturation. To test this, we examined lysosomal maturation in THP-1 macrophages infected with WT and mutant BCG strains by confocal microscopy, using LysoTracker staining to assess lysosomal acidification. We observed that ΔMmpE and MmpE^{NLS1-2} mutants exhibited significantly higher co-localization with LysoTracker compared to WT and Comp-MmpE strains at 24 hpi (Figure 5G), indicating that MmpE suppresses lysosomal maturation during infection. To determine whether this effect is mediated through the PI3K-AKT-mTOR pathway, THP-1 macrophages were treated with the dual PI3K/mTOR inhibitor BEZ235 at concentrations ranging from 0 to 200 nM (Hsu *et al*., 2018). Growth assays confirmed that BEZ235 had no effect on the viability of BCG strains over 8 days (Figure S6A). However, under normal conditions, the ΔMmpE mutant exhibited approximately a 3-fold reduction in intracellular survival compared to the wild-type strain. Upon BEZ235 treatment, this difference in bacterial load was substantially diminished (Figure S6B), suggesting that PI3K-AKT-mTOR signaling contributes to MmpE-mediated immune evasion. We further examined the intracellular survival of WT MmpE, NLS-deleted mutant and phosphatase-inactive strains in THP-1 macrophages treated with 100 nM BEZ235. Under untreated conditions, NLS-deficient and phosphatase-inactive strains exhibited approximately a 2-fold reduction in intracellular survival compared to the WT and complemented MmpE strains. This difference was abolished upon BEZ235 treatment (Figure S6C), further supporting the notion that activation of the PI3K-AKT-mTOR pathway is essential for MmpE-mediated subversion of host antimicrobial responses during mycobacterial infection.

MmpE suppresses the expression of *VDR* during BCG infection

Given the role of MmpE in modulating host signaling pathways, we next investigated whether it directly targets specific host genes during macrophage infection. Focusing on promoter regions (≤1 kb upstream of the transcription start site) of significantly upregulated genes ($|Log_2FC > 1|$ and $P < 0.05$), we identified four candidate transcription factors, including *CREBBP*, *VDR*, *GREB1*, and *FOXP4* (Figure 6A). HOMER *de novo* motif analysis revealed a putative MmpE-binding motif specifically with the promoter of *VDR*, a key anti-inflammatory gene (Aggeletopoulou et al., 2022) (Figure 6B). We next examined *VDR* expression in THP-1 macrophages infected with recombinant strains. Compared to the WT, *VDR* expression was significantly downregulated in cells infected with the ΔMmpE mutant (Figure 6C), suggesting that MmpE suppresses *VDR* transcription. Furthermore, we cloned the *VDR* promoter region (−100 bp to +50 bp) and conducted chromatin immunoprecipitation (ChIP) assays in HEK293T cells. While both *VDR* and *GAPDH* sequences were detected in input controls, *VDR* promoter DNA was selectively detected in ChIP samples from MmpE-EGFP transfected cells (Figure 6D and E). In addition, the DNA-binding capacity of MmpE was unaffected by its phosphatase activity (Figure 7F and G). Electrophoretic mobility shift assays (EMSA) further confirmed the interaction, demonstrating a shifted band corresponding to the MmpE-VDR promoter complex and a dose-dependent increase in complex formation (Figure 7H and I). Collectively, these results suggest that MmpE binds the VDR promoter to modulate its transcription.

To further characterize the MmpE-regulated transcriptional network, we integrated CUT&Tag and RNA-seq data to identify 298 related genes (Table S4; Figure S7A and B). GO enrichment analysis revealed that these genes were significantly enriched in biological processes such as cell differentiation and regulation of small GTPase-mediated signal transduction, both of which are fundamental to immune cell function, trafficking, and inflammatory responses (Li *et al*., 2023; Ma *et al*., 2024) (Figure S7C and D). These findings further establish MmpE as a nucleomodulin that rewires host transcriptional programs involved in immune regulation and cellular defense.

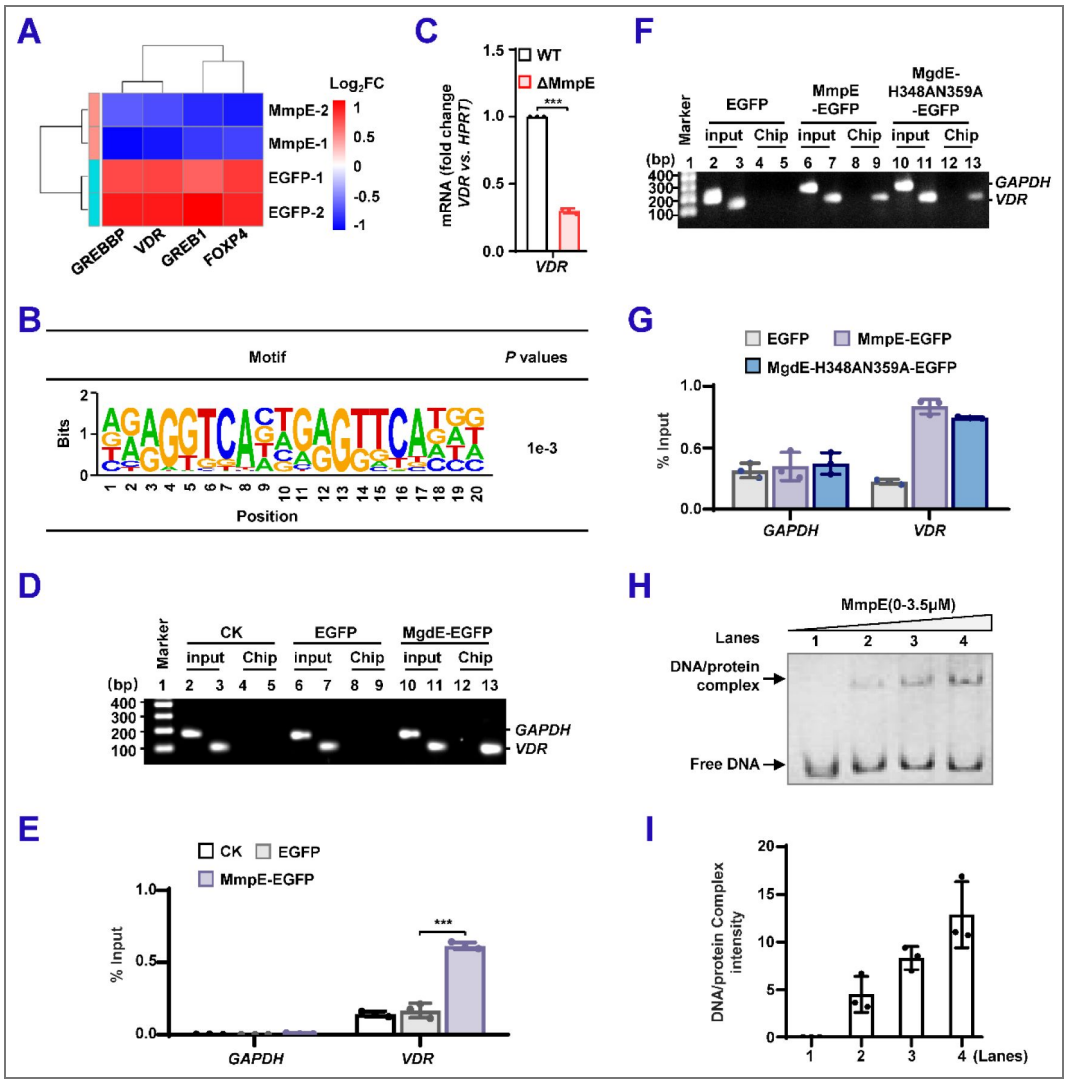

Figure 6. MmpE suppresses the expression of *VDR* during BCG infection

(A) Heatmap of transcription factors associated with MmpE ChIP-seq peaks in HEK293T cells. Color scale indicates expression changes (red: upregulated; blue: downregulated). **(B)** *De novo* motif analysis of MmpE-bound sequences using HOMER. Enrichment P-values were calculated with TOMTOM. "% of targets" indicates the proportion of peaks containing each motif; letter height reflects nucleotide frequency. **(C)** Quantitative RT-PCR analysis of VDR expression in THP-1 cells infected with WT or ΔMmpE strains for 24 h. **(D-G)** ChIP-PCR and qPCR analysis of the *VDR* promoter region. HEK293T cells were transfected with EGFP, MmpE-EGFP, or MmpE- H348A/N359A-EGFP. Chromatin was immunoprecipitated using anti-GFP antibody. PCR was performed with primers targeting the *VDR* promoter and GAPDH (negative control), and products were analyzed by agarose electrophoresis (**D, F**). Enrichment was quantified by qPCR using the $2^{-\Delta Ct}$ method (**E, G**). **(H-I)** EMSA using purified MmpE protein and a DNA probe corresponding to the VDR promoter. Samples were resolved by native PAGE. Arrows indicate the positions of free DNA and slower-migrating species (**H**); signal intensities were quantified by densitometry (**I**). Data represent mean ± SD of three independent biological replicates. Statistical significance determined using two-way ANOVA or two-tailed unpaired Student's *t*-tests, ***$P < 0.001$.

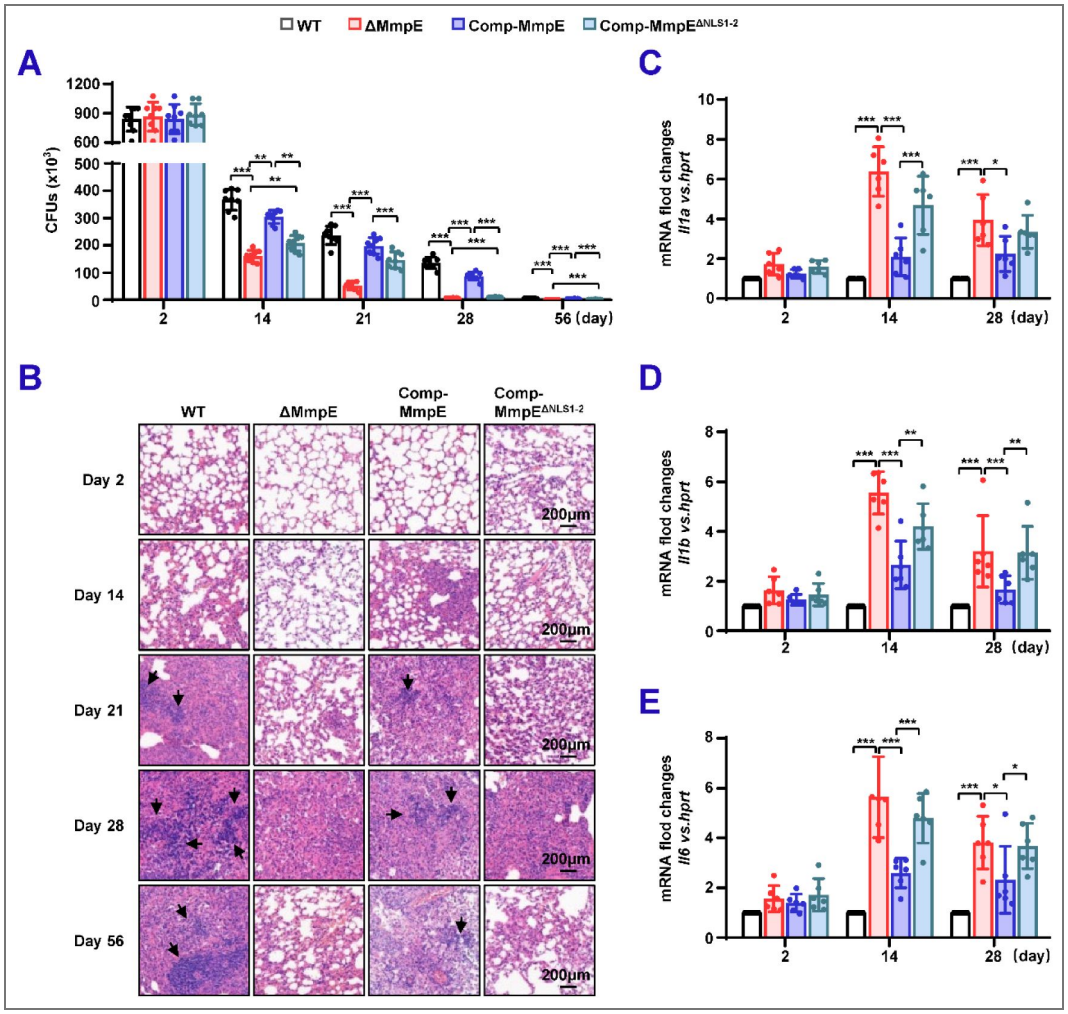

Figure 7. Nuclear translocation of MmpE is essential for mycobacterial survival in mice.

(**A**) Bacterial burden in lungs of infected mice. Specific pathogen-free (SPF) C57BL/6 mice (n = 6 per group) were intranasally infected with 1.0×10^7 CFUs of BCG strains, including WT, ΔMmpE, Comp-MmpE, or Comp-MmpE$^{\Delta NLS1\text{-}2}$. Bacterial titers in lung homogenates were quantified by CFU assays at 0, 14, 28, and 56 dpi. **(B)** Histopathology of infected lung tissues. Hematoxylin and eosin (H&E)-stained lung sections from mice infected as in (**A**) show granulomatous inflammation, Scale bars: 200 μm. **(C-D)** Pro-inflammatory cytokine expression in the spleen of infected mice. qRT-PCR analysis of cytokine mRNA levels of *Il1a* (**C**), *Il1b* (**D**)and *Il6* (**E**) in spleen tissues from infected mice (n = 6/group) at 2 to 28 dpi. Data represent mean ± SD of three independent biological replicates. Statistical significance determined using two-way ANOVA, **P* < 0.05, ***P* < 0.01, ****P* < 0.001.

Nuclear translocation of MmpE is critical for mycobacterial survival in mice

To investigate the role of MmpE as a nucleomodulin in vivo, C57BL/6 mice were infected with WT, ΔMmpE, Comp-MmpE, and Comp-MmpE$^{\Delta NLS1-2}$ strains. Compared with mice infected with WT or Comp-MmpE strains, mice infected with ΔMmpE or Comp-MmpE$^{\Delta NLS1-2}$ strains had significantly lower bacterial loads in their lungs (Figure 7A). Similar results were observed in splenic bacterial colonization (Figure S8A). Hematoxylin and eosin (H&E) staining of lung tissues from the mice infected with WT or Comp-MmpE strains showed extensive inflammatory infiltrates, while the lungs of the mice infected with ΔMmpE or Comp-MmpE$^{\Delta NLS1-2}$ strains exhibited markedly reduced inflammation (Figure 7B). In addition, compared with mice infected with WT or Comp-MmpE strains, mice infected with ΔMmpE or Comp-MmpE$^{\Delta NLS1-2}$ strains showed a significant increase in *Il1a*, *Il1b*, and *Il6* in the spleen (Figure 7C and E). These results indicate that the nuclear translocation of MmpE is critical for mycobacterial intracellular survival.

Since MmpE modulates host transcriptional responses in THP-1 macrophages, we examined the expression of *Vdr*, inflammation-related, and lysosome-associated genes in the lungs and spleens of mice at 14 and 28 days post infection (dpi). *Vdr* expression was significantly reduced in both lungs and spleens infected with the ΔMmpE or Comp-MmpE$^{\Delta NLS1-2}$ strains compared to those infected with WT or Comp-*MmpE* strains (Figure S8B). Consistent with H&E observation, the expression of inflammation-related genes (e.g., *Il23a*, *Csf2*, *Cd69*, *Ido1*, *Il12b*, and *Ceacam1*) were markedly decreased in lungs infected with the ΔMmpE or Comp-MmpE$^{\Delta NLS1-2}$, but significantly elevated in spleens from the same groups (Figure S8C-D). Moreover, as observed in vitro, lysosomal maturation-associated genes, such as *Tfeb*, *Lamp1*, *Lamp2*, together with genes encoding V-ATPase subunits, were upregulated in both lung and spleen tissues of the mice infected with ΔMmpE or Comp-MmpE$^{\Delta NLS1-2}$ (Figure S8E-H). Taken together, our experiments demonstrate that MmpE promotes mycobacterial survival in vivo through its nuclear translocation, likely by modulating host immune responses and lysosomal maturation pathways.

Discussion

MmpE is a bifunctional virulence factor in Mtb

Previously, Forrellad *et al*. (2020) characterized Rv2577/MmpE of Mtb as an alkaline phosphatase/phosphodiesterase that affects phagosome maturation arrest and virulence of Mtb. While the enzymatic activity and virulence-related phenotype of MmpE have been established, specific cofactor dependencies, catalytic residues, and the mechanisms underlying host-pathogen interactions remain inadequately defined. Here, our study shows that MmpE possesses Fe^{3+}-dependent phosphatase activity, with H348 and N359 identified as critical catalytic residues (Figure 2C-E). Moreover, deletion of these residues significantly impairs the survival of recombinant BCG strains in THP-1 macrophages, indicating that its phosphatase activity is essential for intracellular persistence (Figure 3E). Furthermore, our study identifies MmpE as a novel nucleomodulin that translocates into the host nucleus primarily via its nuclear localization signal (NLS; RRK$^{460-462}$) (Figure 1D-G, Figure S1D). Upon infection, MmpE modulates a broad range of host immune signaling pathways, including cytokine-cytokine receptor interactions, TNF, Toll-like receptor, chemokine, NF-κB, JAK-STAT, and PI3K-Akt pathways. Specifically, MmpE enhances the phosphorylation levels of AKT (Ser473), mTOR (Ser2448), and p70S6K (Thr389), modulating the PI3K-AKT-mTOR signaling pathway and ultimately impairing lysosomal maturation to promote intracellular survival of the pathogen (Figure 5E and G, Figure S5C, Figure S6B and C). Additionally, it also regulates the expression of key transcription factors, such as VDR, CREBBP, GREB1, and FOXP4 (Figure 6A). Notably, the deletion of the NLS significantly impairs the functionality of MmpE, thereby reducing the survival of BCG strains in both macrophages and murine models (Figure 3A-D, Figure 7A). Taken together, these findings indicate that MmpE functions as a bifunctional virulence factor, combining phosphatase activity with nuclear localization to modulate host responses during infection.

Targeting host *VDR* gene might represent a unique immune evasion strategy by Mtb

Nucleomodulins are effector proteins secreted by bacterial pathogens that specifically target the host cell nucleus, where they modulate nuclear processes to subvert host responses (Hanford et al., 2021). Their mechanisms of action within the nucleus typically involve indirect interference with host transcriptional programs, such as through epigenetic modifications, chromatin remodeling, or inhibition of key signaling pathways (Jose et al., 2016; Singh et al., 2023). Despite extensive characterization of nucleomodulin functions, direct binding to host gene promoters remains rare and mechanistically distinct. In this study, we found that MmpE directly binds to the promoter of the *VDR* gene (Figure 6) and attenuates the expression of VDR-regulated inflammatory genes (Zhou *et al*., 2020; Yang *et al*., 2019) (Figure 3F-H). VDR is a critical nuclear receptor that controls the expression of numerous genes involved in host immune defense, including antimicrobial peptides and cytokine (Usategui-Martín et al., 2022). For example, Mtb suppresses the expression of the host gene *CYP27B1* to reduce active vitamin D synthesis, thereby limiting VDR activation and downstream antimicrobial responses (Liu et al., 2006). Similarly, *Salmonella* downregulates *VDR* through miRNA-mediated mechanisms, weakening mucosal immunity (Chen et al., 2014). This mechanism of MmpE regulating VDR expression reveals a novel strategy by bacterial pathogens to evade host defenses through direct manipulation of host gene promoters by nucleomodulins.

MmpE regulates the PI3K-Akt-mTOR pathway to inhibit lysosomal maturation and enhance pathogen survival

Mtb employs multiple strategies to evade phagolysosomal degradation, a process essential for bacterial clearance (Chandra et al., 2022; Zhang et al., 2024; Singh and Nagaraja, 2025). For example, approximately 70% of phagosomes harboring Mtb fail to fuse with lysosomes, partly due to the activity of secreted phosphatases such as PtpA, PknG, and SapM, which disrupt vesicular trafficking (Wong et al., 2011; Ge et al., 2022; Zhang et al., 2024; Alsayed and Gunosewoyo, 2024). MmpE has also been shown to contribute to the arrest of lysosomal maturation in human cells; however, the underlying mechanisms remain unclear (Forrellad et al., 2020).

In this study, we elucidate a mechanism by which MmpE inhibits lysosomal maturation. The absence of MmpE during BCG infection resulted in substantial upregulation of lysosome-associated genes, including *TFEB*, a master regulator of lysosomal biogenesis and function, underscoring MmpE's role in lysosomal regulation (Jeong *et al*., 2021; Wang *et al*., 2024) (Figure 4G, Figure S4C). Moreover, the ΔMmpE and MmpE$^{\Delta NLS1\text{-}2}$ mutants exhibited significantly increased expression of lysosomal maturation-associated genes in both mice and infected THP-1 cells, along with enhanced LysoTracker co-localization in THP-1 cells, compared to WT and Comp-MmpE strains (Figure 4G, Figure 5G, Figure S8C-F). Collectively, these findings indicate that MmpE inhibits lysosomal maturation during mycobacterial infection. Furthermore, CUT&Tag analysis revealed that MmpE binds to the promoter regions of host genes within the PI3K-Akt-mTOR signaling pathway, including *PRKCB*, *PLCG2*, and *PIK3CB*, which are key upstream regulators of TFEB activity (Fang et al., 2021; Gounis et al., 2025) (Figure S5A). Additionally, during infection, WT strains exhibited significantly elevated phosphorylation of Akt, mTOR, and p70S6K compared to the ΔMmpE and the Comp-MmpE$^{\Delta NLS1\text{-}2}$ strain (Figure 5E-F, Figure S5C). When THP-1 macrophages were treated with the dual PI3K/mTOR inhibitor BEZ235, the survival difference between WT and MmpE mutants was significantly reduced (Figure S6B-C). These results collectively indicate that MmpE regulates the PI3K-Akt-mTOR-TFEB axis, thereby inhibiting lysosomal maturation and enhancing bacterial survival in the host.

In summary, our study identifies MmpE as a novel bifunctional virulence factor of mycobacteria, combining Fe^{3+}-dependent phosphatase activity with nuclear translocation capability. MmpE translocates into the host nucleus and directly binds to the promoters of some key host genes, such as *VDR*, thereby inhibiting the expression of the downstream targets implicated with the inflammation responses and lysosomal maturation, thereby promoting mycobacterial survival in

macrophages and in mice (Figure 8). These findings reveal a sophisticated mechanism by which bacterial pathogen manipulates host gene transcription and signaling pathway to promote intracellular persistence.

Materials and methods

Bacterial strains and culture conditions

The bacterial strains used in this study are detailed in Table S6. *E. coli* DH5α and BL21 were cultured in Luria-Bertani (LB) medium under standard conditions. *M. bovis* BCG strains were grown in Middlebrook 7H9 broth supplemented with 10% (v/v) OADC (oleic acid, albumin, dextrose, catalase), 0.05% (v/v) Tween-80, and 2% (v/v) glycerol. Antibiotics were added as required at the following final concentrations: 50 μg/mL hygromycin (for mycobacteria) and 50 μg/mL kanamycin (for both mycobacteria and *E. coli*).

Cell culture

THP-1 cells were cultured in Roswell Park memorial institute 1640 (RPMI 1640) medium supplemented with 10% (v/v) heat-inactivated fetal bovine serum (FBS), 1 mM sodium pyruvate, 2 mM L-glutamine, 10 mM HEPES buffer (pH 7.2-7.5), and 50 μM 2-mercaptoethanol. For differentiation into macrophages, THP-1 cells were treated with 200 nM phorbol 12-myristate 13-acetate (PMA) for 24 h to allow complete differentiation prior to experimental use.

HEK293T cells and RAW264.7 macrophages were cultured in Dulbecco's modified Eagle's medium (DMEM) supplemented with 10% (v/v) FBS and 50 μg/mL penicillin-streptomycin. All cells were maintained at 37 °C in a humidified atmosphere with 5% CO_2.

Animal experiments

Specific pathogen-free (SPF) female C57BL/6 mice (6-8 weeks old, 16-18 g) were obtained from Chang-sheng Bio (Liaoning, China). All animals were maintained under SPF conditions in individually ventilated cages with controlled temperature and humidity, on a 12-hour light/dark cycle. Mice had ad libitum access to sterilized food and water.

Phylogenetic and sequence analysis

Homologs of the metallophosphatase MmpE were identified from 11 *Mycobacterium* species, including *M. tuberculosis* (Mtu), *M. bovis* BCG (Mbb), *M. orygis* (Mory), *M. kubicae* (Mku), *M. paraterrae* (Mpa), *M. farcinogenes* (Mfg), *M. mucogenicum* (Mmuc), *M. vicinigordonae* (Mvg), *M. lentiflavum* (Mlf), *M. avium* (Mav), and *M. manitobense* (Mman). Genomic sequences were retrieved from the NCBI RefSeq database and filtered for completeness.

Protein sequences were aligned using Clustal Omega v1.2.4 with default parameters (gap opening penalty = 10, gap extension = 0.2, and iterative refinement enabled). Conserved residues (≥90% identity) were visualized using ESPript 3.0. Phylogenetic reconstruction was performed in MEGA v12.0 using the neighbor-joining algorithm with pairwise deletion for gap treatment and a Poisson substitution model, appropriate for closely related bacterial sequences. Bootstrap support was calculated with 1,000 replicates, and nodes with values ≥50% were retained. The resulting tree was visualized using the iTOL platform, without additional pruning.

Structural Analysis of MmpE

Structural models of full-length MmpE and its NLS-deletion mutants ($MmpE^{\Delta NLS1}$, $MmpE^{\Delta NLS2}$, $MmpE^{\Delta NLS1\text{-}2}$) were generated using AlphaFold v2.2.0. Predictions were performed with default settings, including use of the pre-trained model and MSA generation via UniRef90 and MGnify. Model confidence was assessed using pLDDT scores. All structures were analyzed in UCSF ChimeraX for conformational differences between mutants. The AlphaFold-predicted reference model was further examined in PyMOL to identify putative metal-binding residues based on spatial proximity and coordination geometry within the predicted active site.

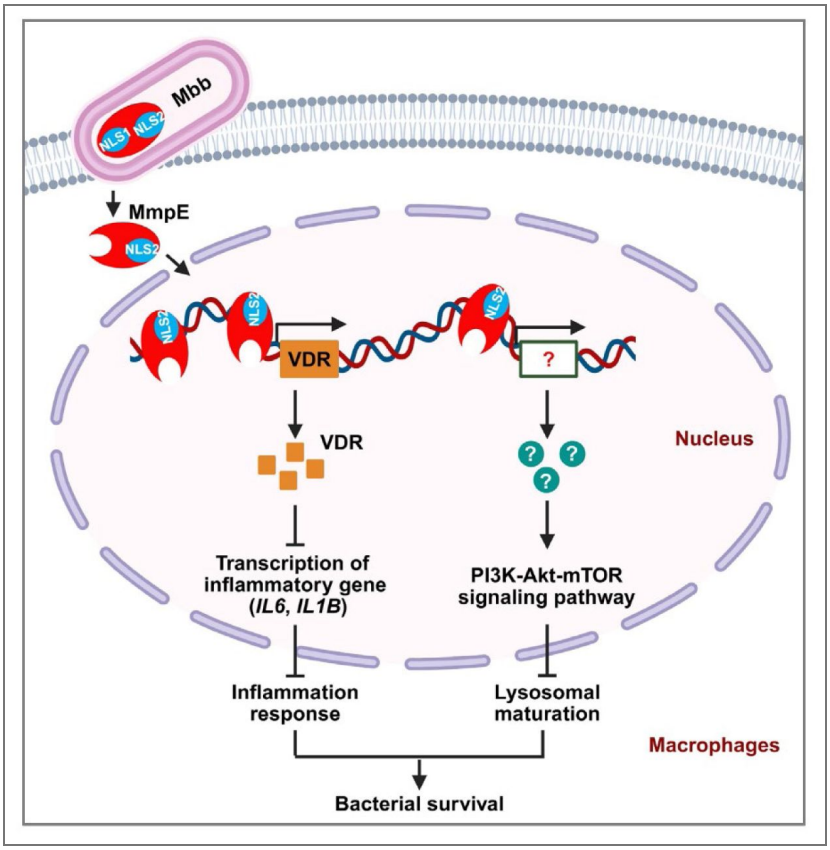

Figure 8. Schematic diagram of nucleomodulin MmpE-mediated immune suppression and enhanced mycobacterial survival.

During infection, the nucleomodulin MmpE translocates into the host nucleus via its C-terminal NLS2 motif ($RRK^{460\text{-}462}$), where it binds to the VDR promoter and suppresses transcription of inflammatory genes. Simultaneously, MmpE regulates the PI3K-Akt-mTOR signaling pathway, thereby inhibiting lysosome maturation. These dual mechanisms contribute to immune evasion and promote intracellular survival of mycobacteria.

Cell transfection and confocal microscopy

HEK293T cells were seeded at 70% confluency in poly-L-lysine-coated 35-mm glass-bottom dishes and maintained in DMEM supplemented with 10% (v/v) FBS at 37 °C with 5% CO_2. Transfection was performed using the Hieff Trans™ Liposomal Transfection Reagent according to the manufacturer's protocol. Briefly, 0.5 μg of plasmid DNA and 1.5 μL of transfection reagent were diluted in 250 μL of Opti-MEM, incubated at room temperature for 20 minutes, and added dropwise to each well.

At 24-48 hpt, cells were washed with PBS, fixed in 4% paraformaldehyde for 15 min, and permeabilized with 0.1% Triton X-100 for 10 min. Nuclei were counterstained with 1 μg/mL DAPI for 10 min. Imaging was performed using an Olympus FV1000 Confocal Laser Scanning Microscope equipped with a 100×/1.40 NA oil immersion objective. Fluorescence was detected using the following parameters: EGFP, excitation at 488 nm, emission at 509 nm; DAPI, excitation at 405 nm, emission at 461 nm. Spectral unmixing was applied using FV10-ASW v4.2 to minimize channel cross-talk. Z-stack images were acquired in sequential mode with a step size of 0.5 μm to ensure consistency across samples.

Cell fractionation and Immunoblotting

Cells were lysed in RIPA buffer supplemented with 1 % (v/v) protease inhibitor cocktail, and protein concentrations were determined using the BCA assay. Equal amounts of protein were separated by SDS-PAGE and transferred onto PVDF membranes. Membranes were blocked for 1 h at room temperature with 5% (w/v) non-fat milk in TBST (25 mM Tris, 150 mM NaCl, 2 mM KCl, 0.2% Tween-20, pH 7.4), then incubated overnight at 4 °C with primary antibodies. After three 6-min washes with TBST, membranes were incubated with HRP-conjugated secondary antibodies for 1 h at room temperature. Signal detection was performed using enhanced chemiluminescence (ECL), and images were acquired with the ChemiDoc™ MP Imaging System (Bio-Rad). For subcellular fractionation, nuclear and cytoplasmic protein fractions were prepared using the Nuclear and Cytoplasmic Protein Extraction Kit (Beyotime) with minor modifications. Cells were washed with PBS, detached using a cell scraper, and pelleted by centrifugation at 2,000 × *g* for 5 min. The pellet (~20 μL packed cells) was resuspended in 150 μL of Cytoplasmic Extraction Reagent A (with PMSF), vortexed for 5 s, and incubated on ice for 15 min. After addition of 10 μL Reagent B, the sample was vortexed briefly, incubated on ice, and centrifuged at 12,000 × *g* for 5 min at 4 °C to collect the cytoplasmic fraction (supernatant). The remaining pellet was extracted with 50 μL of Nuclear Extraction Reagent (with PMSF), vortexed intermittently for 30 min on ice, and centrifuged at 12,000 × *g* for 10 min at 4 °C to obtain the nuclear fraction. β-actin, or histone H3 was used as a loading control for cytoplasmic or nuclear fractions. Antibody information is listed in the Table S1.

Immunoblot analysis of MmpE secretion

The procedure for immunoblot analysis of MmpE secretion was adapted from previous studies with minor modifications (Zhang et al., 2022; Chen et al., 2025). BCG strains expressing C-terminally Flag-tagged MmpE were cultured in Middlebrook 7H9 broth with 0.5% glycerol, 0.02% Tyloxapol, and 50 μg/mL kanamycin at 37 °C (80 rpm) until OD600 ~0.6. Cells were harvested by centrifugation (4,000 × *g*, 15 min, 4 °C), and supernatants filtered through 0.22 μm PES membranes. Filtrates were concentrated ~50-fold using Amicon Ultra-15 filters (10 kDa cutoff) for secreted MmpE detection. Bacterial pellets were washed, resuspended in lysis buffer (50 mM Tris-HCl, pH 7.5; 150 mM NaCl; 1 mM PMSF; protease inhibitors). Lysates were clarified by centrifugation (10,000 × *g*, 15 min, 4 °C). Whole-cell lysates and concentrated culture filtrates were analyzed by immunoblotting as described above, using anti-Flag antibodies for detection.

Protein Expression and Purification

N-terminal maltose-binding protein (MBP)-tagged and C-terminal His_6-tagged wild-type MmpE, as well as mutant lacking the Tat signal peptide were expressed in *E. coli* BL21 (DE3). Protein expression was performed in 1 L of LB medium. Cultures were grown at 37 °C until the optical density at 600 nm (OD_{600}) reached approximately 0.8, after which protein expression was induced with 0.2 mM IPTG at 18 °C for 24 h. Following induction, cells were harvested by centrifugation and lysed by sonication in ice-cold lysis buffer containing 150 mM NaCl, 30 mM Tris-HCl (pH 7.5), and 1 mM PMSF. The lysate was clarified by centrifugation, and the supernatant was subjected to affinity purification using an MBP affinity column.

Phosphatase activity assay

Phosphatase activity was measured using *p*-nitrophenyl phosphate (*p*-NPP) as the substrate in a final reaction volume of 200 µL. Reactions were initiated by incubating 0-80 µg of purified protein with *p*-NPP at 37 °C for 60 min. The release of *p*-nitrophenol (*p*-NP), the dephosphorylated product, was quantified by measuring absorbance at 405 nm using a microplate spectrophotometer.

Kinetic parameters were determined under initial velocity (V_0) conditions using substrate concentrations ranging from 0.1 to 10 mM *p*-NPP. The kinetic constants Km and Vmax were calculated by fitting the data to the Michaelis-Menten equation using nonlinear regression analysis in GraphPad Prism 8.0. The catalytic turnover rate (Kcat) was calculated using the equation Kcat = $Vmax/E_o$, where Vmax was expressed as nM *p*-NP min^{-1} and E_0 represents the active enzyme concentration. Control reactions were carried out in the absence of either the substrate or the enzyme to measure background absorbance. All assays were performed in triplicate to ensure the reproducibility of results.

Quantitative real-time PCR

THP-1 cells were infected with the BCG strain and harvested 24 hpi for total RNA isolation. RNA was extracted using 1 mL of TRIzol® reagent following the manufacturer's protocol. To eliminate genomic DNA contamination, RNA samples were treated with DNase I for 30 min at 37 °C, followed by heat inactivation at 65 °C for 10 min. RNA concentration and purity were assessed using a NanoDrop 2000 spectrophotometer (Thermo Fisher Scientific).

For cDNA synthesis, 1 µg of total RNA was reverse transcribed using the HiScript® III cDNA Reverse Transcription Kit with random hexamers primers, according to the manufacturer's protocol. qRT-PCR was performed using ChamQ SYBR® Green RT-PCR Master Mix. Relative mRNA expression levels were calculated using the $2^{-\Delta\Delta Ct}$ method, normalizing Ct values to the housekeeping gene *HPRT*. All qRT-PCR experiments were conducted in triplicate, with at least three independent biological replicates and two technical replicates per condition. Primer sequences are listed in Table S7.

RNA-seq analysis

THP-1 cells were seeded at a density of 1×10^6 cells well in 6-well plates and differentiated into macrophages by treatment with 100 nM PMA for 48 h. After differentiation, cells were washed with PBS and infected with BCG WT or ΔMmpE strains at a multiplicity of infection (MOI) of 10:1. Following 24 h of infection, total RNA was extracted using TRIzol® reagent according to the manufacturer's protocol.

High-quality sequencing reads were then aligned to the human reference genome (GRCh38) using HISAT2 (v2.2.1). Transcript quantification was performed using FeatureCounts (v2.0.3), and differential gene expression analysis was conducted using DESeq2 (v1.38.3) in R. Genes with an adjusted *P*-value < 0.05 and an absolute $|\log_2$ fold change ≥ 1| were considered significantly differentially expressed. RNA-seq data were visualized using GraphPad Prism version 8.0, as well as volcano plots, heatmaps, and other graphical outputs generated via the SRplot platform (Tang et al., 2023).

CUT&Tag analysis

HEK293T cells were seeded in 10 cm² dishes at a density of 1 × 10^7 cells per well and transfected with 10 μg of the MmpE-pEGFP expression plasmid using Hieff Trans™ Liposomal Transfection Reagent, following the manufacturer's instructions. Cells transfected with the empty vector pEGFP-N1 were used as controls. At 36 hpt, cells were collected for CUT&Tag analysis. For the CUT&Tag, cells were fixed with 1% formaldehyde at room temperature for 10 min, and the reaction was quenched with 0.125 M glycine. After centrifugation, cells were permeabilized using ice-cold wash buffer containing 0.05% digitonin. Primary antibody incubation was carried out overnight at 4 °C using mouse anti-GFP antibody (1:1000), followed by a 2 h incubation at room temperature with Protein A/G-conjugated secondary antibody (1:100). Cells were then incubated at 37 °C for 1 h with a Protein A-Tn5 transposase complex (1:100) preloaded with Illumina sequencing adapters.

The reaction was terminated using lysis buffer containing 10% SDS, followed by proteinase K digestion. DNA was purified and amplified by PCR (12 cycles) using the NEBNext Ultra II DNA Library Preparation Kit. Fragment size distribution (150-300 bp) was confirmed using the Agilent 2100 Bioanalyzer. Sequencing was performed on the Illumina NovaSeq 6000 platform, producing 150 bp paired-end reads. Raw reads were quality-checked using FastQC and aligned to the human reference genome (hg38). Peak calling was conducted using MACS2 (v2.2.7) with the parameters --nomodel -- qvalue 0.05. Genomic annotation, GO analysis, and *de novo* motif discovery were performed using HOMER (v4.11). Identified motifs were matched to known transcription factor binding motifs using TOMTOM, with a statistical significance threshold of $p < 0.001$.

Chromatin Immunoprecipitation (ChIP) assays

ChIP assays were performed to validate the direct binding of MmpE to the promoter regions of target genes. HEK293T cells were transfected with either EGFP, or MmpE-EGFP expression plasmids. Cross-linking, chromatin isolation, fragmentation, and immunoprecipitation were carried out following the same procedure described for the CUT&Tag assay. DNA was purified from both input and immunoprecipitated (IP) samples and subjected to PCR using primers specific to the promoter regions of the target genes (-100 bp to +50 bp relative to the transcription start site). *GAPDH* primers were used as a negative control. PCR products were analyzed by agarose gel electrophoresis. For quantitative analysis, ChIP-qPCR was carried out using the same primer sets. All reactions were performed in triplicate. Relative enrichment was calculated using the $2^{-\Delta Ct}$ method with normalization to input DNA.

Electrophoretic mobility shift assays (EMSA)

DNA substrates were amplified by PCR from the genomic DNA of *Mycobacterium tuberculosis* H37Rv. The sequences of the oligonucleotide fragments used in the assay are listed in Table S7. EMSA was carried out using a modified protocol as previously described (Li *et al.*, 2020). Each 20 μL reaction contained PCR-amplified DNA fragments, purified MmpE protein at varying concentrations, and binding buffer composed of 20mM Tris-HCl (pH 8.0), 50mM KCl, 50mM $MgCl_2$, 0.2 mM $NiSO_4$, 0.05 mg/mL bovine serum albumin (BSA), 1mM DTT, 10% (v/v) glycerol. Reaction mixtures were incubated on ice for 30 minutes to allow protein-DNA complex formation. Samples were then resolved on a 4.8% native polyacrylamide gel using a running buffer containing 15 mM Tris-HCl (pH 7.5), 0.1 M glycine, 1mM DTT, 50 μM $MgCl_2$ and 0.2 μM $NiSO_4$ at 80 V. Following electrophoresis, gels were stained with ethidium bromide and visualized using a Gel Imaging Analysis System (JIAPENG, China).

Detection of Phagosomal Acidification

THP-1 cells were seeded at 70% confluency in poly-L-lysine-coated 35-mm glass-bottom dishes and maintained in RPMI 1640 supplemented with 10% (v/v) FBS and 200 nM PMA for 24 h at 37 °C under 5% CO_2. After two washes with PBS, the cells were infected with DiD-labeled BCG strains at a MOI of 10 for 24 h, LysoTracker was added for 1 h, followed by Hoechst staining for 15 minutes to visualize the nuclei. Hoechst staining was excited at 350 nm and emitted at 461 nm (blue), while

LysoTracker was excited at 504 nm and emitted at 511 nm (green); DiD was excited at 644 nm and emitted at 665 nm (red). Image analysis was performed by calculating the percentage co-localization of LysoTracker with the phagosomes to assess the effects of different mutants.

Colony-Forming Unit (CFU) assay

For bacterial preparation, mid-log phase cultures of BCG (OD_{600} = 0.6) were harvested, washed with PBS, and resuspended in fresh medium. THP-1 cells were seeded in 12-well plates at a density of 5×10^5 cells per well and and differentiated into macrophage-like cells by treatment with 100 nM PMA for 24 h. After differentiation, cells were washed with PBS and treated with the PI3K-Akt-mTOR pathway inhibitor BEZ235 at various concentrations (0-200 nM). BEZ235 was applied with bacterial infection (co-treatment). An equivalent volume of DMSO was used as a vehicle control for all treatment conditions.

Cells were infected at a MOI of 10:1 and incubated for 4 h. After infection, extracellular bacteria were removed by treatment with penicillin-streptomycin (100 μg/mL) for 4 h. Cells were then washed three times with PBS and maintained in antibiotic-free medium until harvest. Intracellular bacterial burdens were assessed at multiple time points post-infection, macrophages were lysed with 0.25% SDS for 10 minutes at room temperature. Lysates were serially diluted in PBS, and 100 μL aliquots of each dilution were plated on Middlebrook 7H10 agar supplemented with 10% OADC and kanamycin (50 μg/mL). Plates were incubated at 37 °C for 14 days. CFUs were enumerated, and final counts were calculated by applying the corresponding dilution factors. BCG strains used in this study are listed in Table S6.

Mice infection

Mice were infected as described previously (Chen et al., 2022), with minor modifications. Mid-log phase BCG cultures were washed twice in PBS containing 0.05% Tween 80 and briefly sonicated to disrupt bacterial clumps. Female C57BL/6 mice were anesthetized with isoflurane and intranasally inoculated with 1×10^7 CFUs of BCG in 40 μL of PBS. To confirm the inoculation dose, six mice were euthanized at 48 hpi. Lungs were harvested, homogenized in 1 mL of PBS using a tissue homogenizer, and serial dilutions of the homogenates were plated on Middlebrook 7H10 agar supplemented with 10% OADC. Plates were incubated at 37 °C with 5% CO_2 for 14 days, after which CFUs were enumerated.

Histological analysis

Lung tissues from BCG-infected mice were fixed in 4% phosphate-buffered formalin at room temperature for 24 h, followed by paraffin embedding. Paraffin-embedded tissue samples were sectioned into 2-3 μm thick slices using a microtome. Sections were deparaffinized, rehydrated through a graded ethanol series, and stained with hematoxylin and eosin (H&E). Stained tissue sections were examined using an Olympus BX53 light microscope. For digital analysis and annotation, scanned slides were visualized using CaseViewer software (version 2.0; 3DHISTECH).

Ethics approval

All animal experiments were conducted in accordance with the protocols approved by the Animal Ethics Committee of the Huazhong Agricultural University.

Statistical analyses

Data are presented as mean ± standard deviation (SD). Statistical comparisons were performed using two-tailed unpaired Student's *t*-tests or two-way ANOVA. A *P*-value of less than 0.05 was considered significant, with significance levels indicated as follows: $P < 0.05$ (*), $P < 0.01$ (**), and $P < 0.001$ (***). All statistical analyses were performed using GraphPad Prism (version 8.0). Data were obtained from at least three independent biological replicates, each including two or more technical replicates.

Supplementary figures

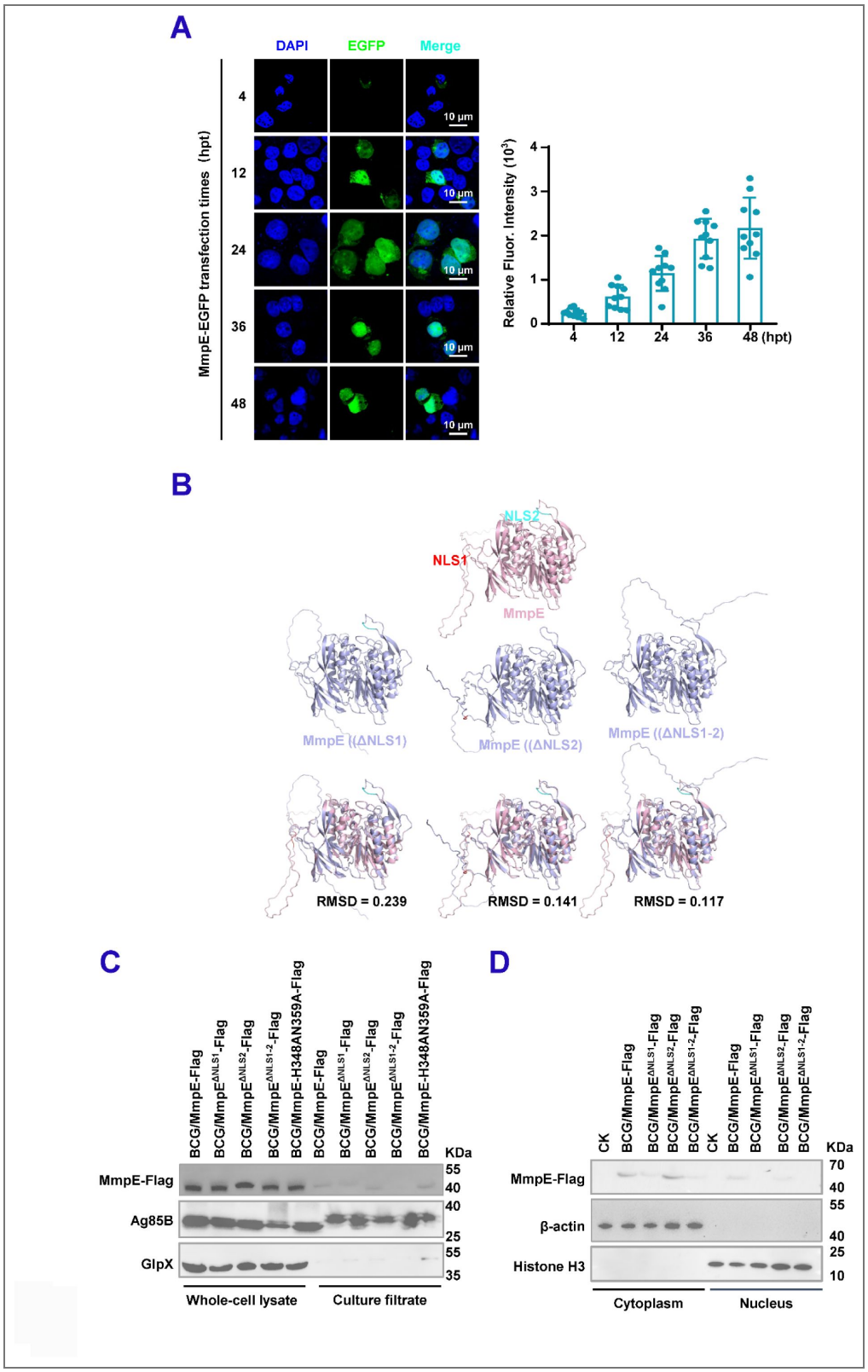

Supplementary Figure 1. Identification of MmpE as a nucleomodulin in Mycobacterium. (**A**) Subnuclear distribution of MmpE-EGFP in transfected cells. Confocal microscopy was performed at indicated time points post-transfection. Nuclei were stained with DAPI (blue); MmpE-EGFP is shown in green. Scale bar, 10 μm. (**B**) Structural modeling of MmpE and NLS mutants. Predicted structures of wild type MmpE, NLS-deletion construct, and

mutants lacking NLS1, NLS2, or both were generated using AlphaFold2. Models were visualized with UCSF ChimeraX, and prediction confidence was evaluated using pLDDT scores. **(C)** Immunoblot analysis of MmpE-Flag expression in bacterial lysates and culture supernatants from recombinant BCG strains. Ag85B and GlpX served as positive and negative controls for secretion, respectively. MmpE-Flag was detected with anti-Flag antibody. **(D)** Subcellular distribution of MmpE during infection. THP-1 macrophages were infected for 24 h with recombinant BCG strains expressing Flag-tagged wild-type MgdE or NLS-deletion mutants ($MmpE^{\Delta NLS1}$, $MmpE^{\Delta NLS2}$, and $MmpE^{\Delta NLS1-2}$). Cytoplasmic and nuclear fractions were prepared and analyzed by immunoblotting using anti-Flag antibody. Histone H3 and β-actin were included as nuclear and cytoplasmic markers, respectively.

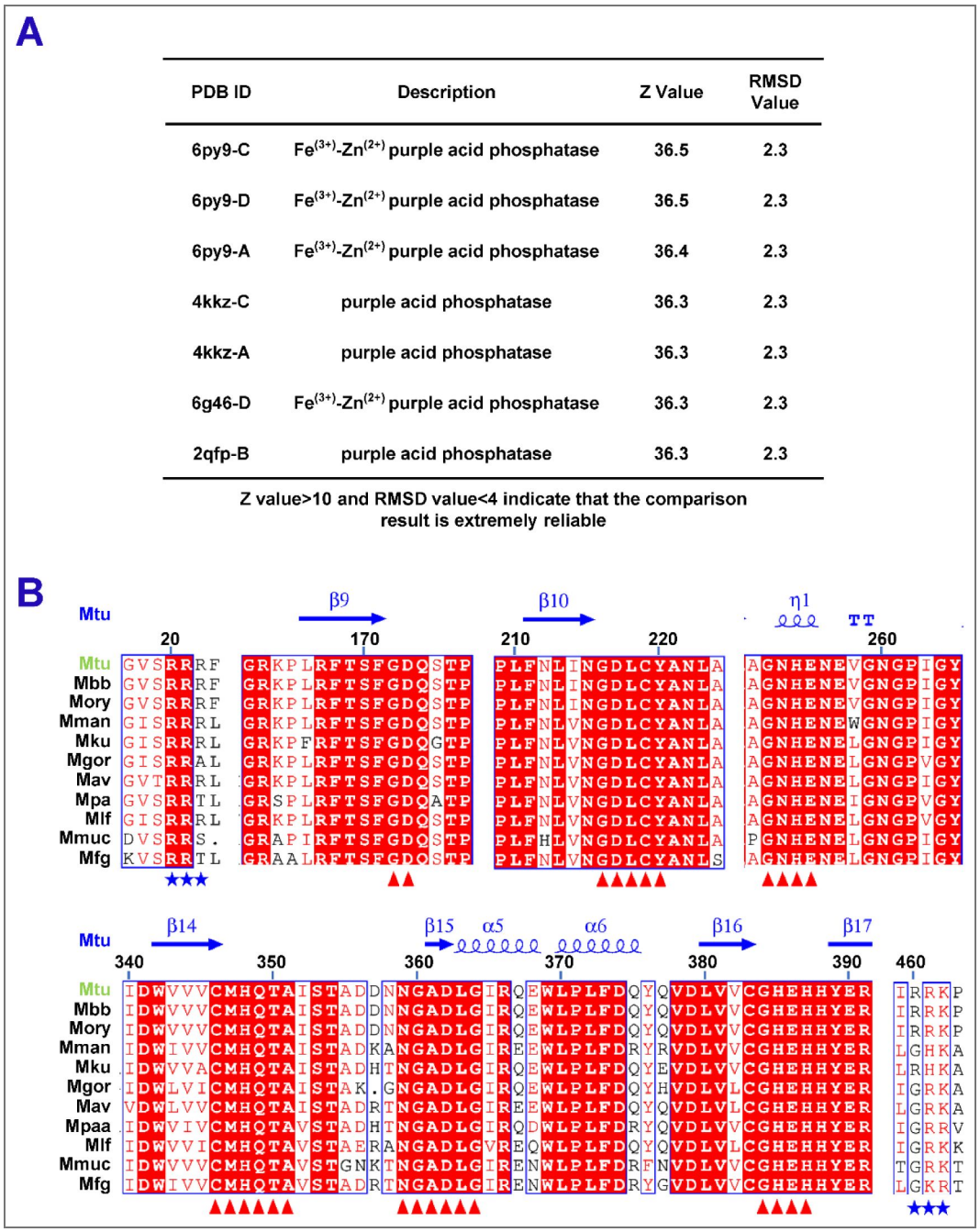

Supplementary Figure 2. Identification of MmpE as a conserved Fe^{3+}/Zn^{2+}- metallophosphatase in Mycobacteria.

(A) Sequence and structure-based analyses of MmpE. UCSF Chimera was used to analyze conserved domains and structural features. Structural similarity was evaluated by comparison with known metallophosphatases. Alignments with *Z*-scores >10 and RMSD <4 were considered high-confidence matches. **(B)** Clustal Omega sequence alignment of MmpE from various mycobacterial species, highlighting conserved residues (≥90% identity, shown in red). Blue stars indicate the predicted NLSs, and red triangles mark characteristic sequences found in metallophosphatases. Species abbreviations: *M. tuberculosis* (Mtu), *M. bovis* BCG (Mbb), *M. orygis* (Mory), *M. kubicae* (Mku), *M. paraterrae* (Mpa), *M. farcinogenes* (Mfg), *M. mucogenicum* (Mmuc), *M. vicinigordonae* (Mgor), *M. lentiflavum* (Mlf), *M. avium* (Mav), *M. manitobense* (Mman).

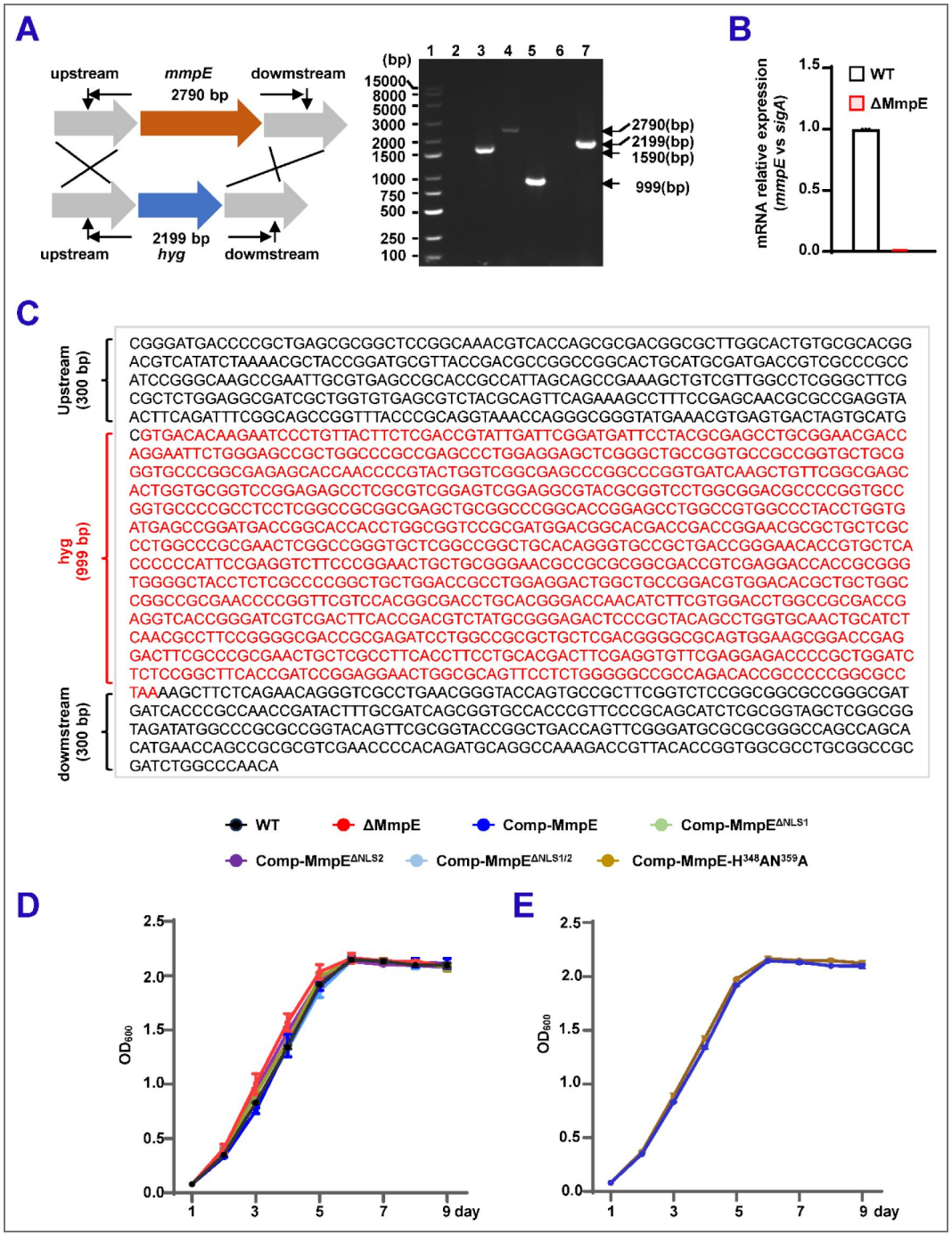

Supplementary Figure 3. The nuclear translocation and phosphatase activity of MmpE are essential for *M. bovis* BCG survival in macrophage cells.

(**A**) Construction and validation of the MmpE-deleted strain of BCG. (left) Schematic diagram of the homologous recombination strategy used to delete *mmpE* from the BCG genome. (right) Wild-type and ΔMmpE strains were used as templates to amplify the *mmpE* gene (600 bp upstream-600 bp downstream) by PCR. Lanes 1 and 3: wild-type genomic DNA; lanes 2 and 4: ΔMmpE genomic DNA. (**B**) qRT-PCR detected the *mmpE* expression level in WT and ΔMmpE strains. **(C)** Sequencing results of ΔMmpE genomic DNA. The forward primer amplified a 300 bp upstream fragment, and the reverse primer a 300 bp downstream fragment. (**D-E**) Growth curve analysis of BCG strains. Strains including WT, ΔMmpE, Comp-MmpE, Comp-MmpE$^{\Delta NLS1}$, Comp- MmpE$^{\Delta NLS2}$, Comp-MmpE$^{\Delta NLS1\text{-}2}$ strains(**C**), or Comp-MmpE-H348AN359H (**D**), were measured in 7H9 medium. Data represent mean ± SD of three independent biological replicates. Statistical significance determined using two-way ANOVA, **P* < 0.05, ***P* < 0.01, ****P* < 0.001.

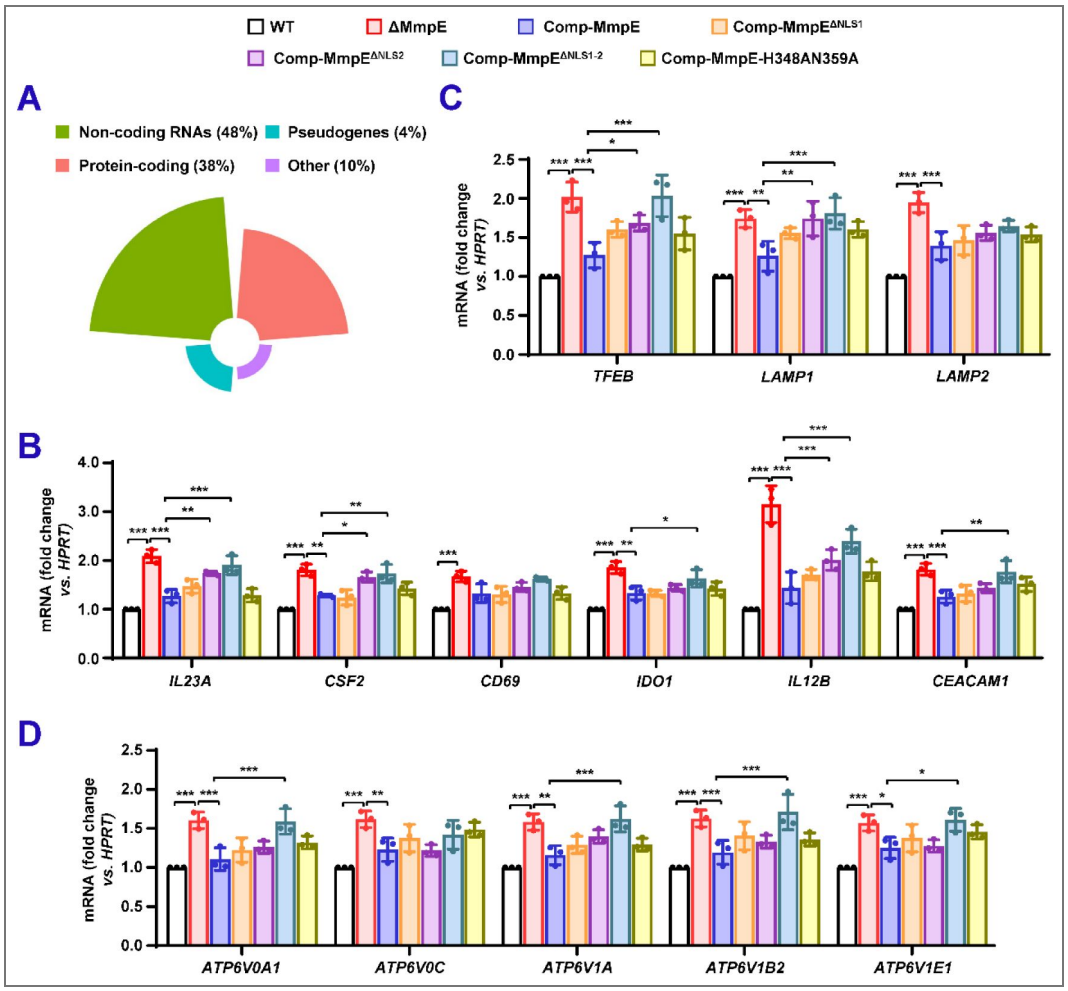

Supplementary Figure 4. MmpE modulates host transcription network involved in inflammation response and lysosomal maturation

(**A**) Biotype distribution of potential MmpE-regulating DEGs in THP-1 cells. (**B-D**) Quantitative RT-PCR analysis of gene expression in infected THP-1 cells. Cells were infected with WT, ΔMmpE, Comp-MmpE, Comp-MmpE$^{\Delta NLS1}$, Comp-MmpE$^{\Delta NLS2}$, Comp-MmpE$^{\Delta NLS1-2}$ and Comp-MmpE-H348AN359H strains for 24 hpi. Cytokine-related genes (*IL23A*, *CSF2*, *CD69*, *IDO1*, *IL12B*, *CEACAM1*) (**B**); genes associated with lysosomal maturation (*TFEB*, *LAMP1*, *LAMP2*) (**C**); genes encoding V-ATPase subunits (*ATP6V0A1*, *ATP6V0C*, *ATP6V1A*, *ATP6V1B2*, and *ATP6V1E1*) (**D**). Data represent mean ± SD of three independent biological replicates. Statistical significance determined using two-way ANOVA, **P* < 0.05, ***P* < 0.01, ****P* < 0.001.

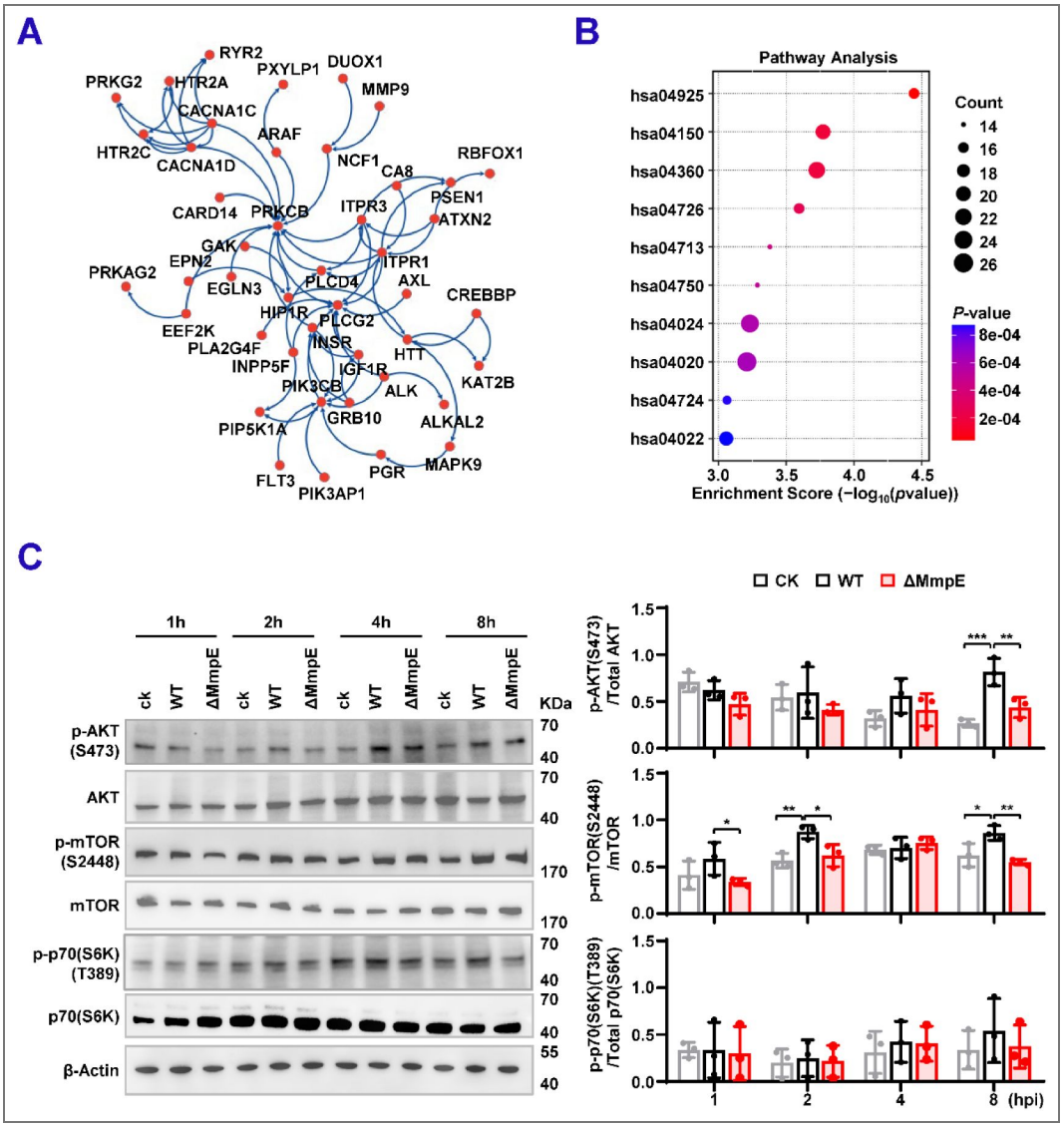

Supplementary Figure 5. MmpE regulates the PI3K-Akt-mTOR signaling pathway during macrophage infection.

(A) Interaction network of DEGs associated with MmpE-binding sites. The network was constructed using STRING v12.0 and visualized with Cytoscape. **(B)** KEGG pathway enrichment analysis of MmpE-binding sites identified in MmpE-EGFP-transfected HEK293T cells. Selected significantly enriched pathways are shown. Bar length indicates the number of associated genes; color represents -$\log_{10}$(*P*-value). Enriched pathways include aldosterone-regulated sodium reabsorption (hsa04925), mTOR signaling (hsa04150), axon guidance (hsa04360), serotonergic synapse (hsa04726), circadian entrainment (hsa04713), inflammatory mediator regulation of TRP channels (hsa04750), cAMP signaling (hsa04024), calcium signaling (hsa04020), glutamatergic synapse (hsa04724), and cGMP-PKG signaling (hsa04022). **(C)** (left) Immunoblot analysis of PI3K-Akt-mTOR pathway activation in THP-1 macrophages infected with either wild-type (WT) or ΔMmpE strains. Phosphorylation of Akt (Ser473), mTOR (Ser2448), and p70S6K (Thr389) was assessed at 0, 2, 4, and 8 hpi. (right) Quantification of phosphorylation levels across time points. Data represent mean ± SD of three independent biological replicates. Statistical significance determined using two-tailed unpaired Student's *t*-tests, $*P < 0.05$, $**P < 0.01$.

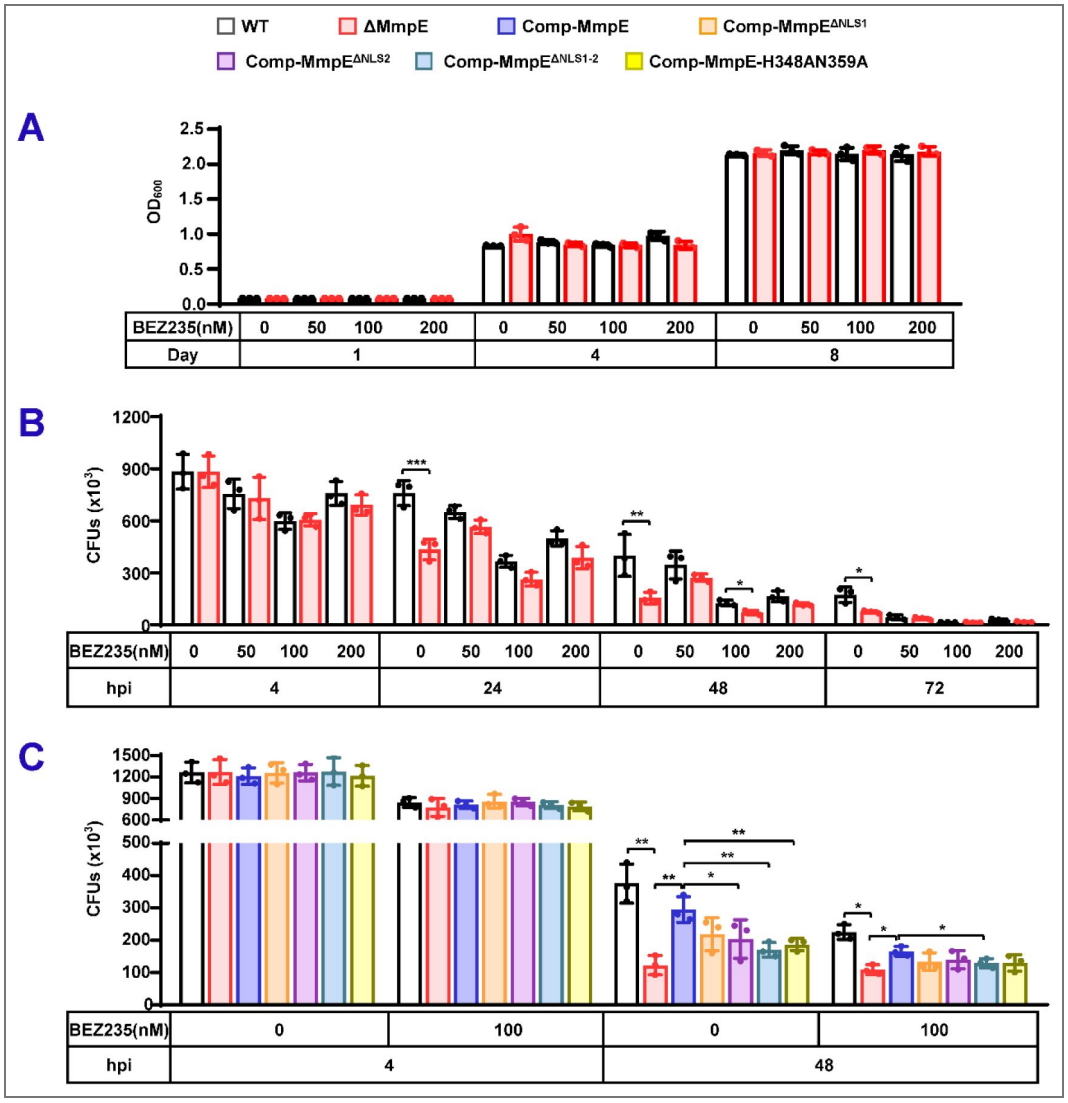

Supplementary Figure 6. MmpE promotes pathogen intracellular survival via the PI3K-Akt-mTOR signaling pathway.

(A-C) Effects of BEZ235 on the growth and intracellular survival of BCG strains. Bacterial growth in 7H9 medium with or without BEZ235 (0-200 nM) (**A**). Intracellular survival of WT and ΔMmpE strains in THP-1 macrophages treated with or without BEZ235 (0-200 nM); CFUs were quantified at 48 hpi (**B**). Intracellular survival of WT, ΔMmpE, Comp-MmpE, Comp-MmpE$^{\Delta NLS1}$, Comp-MmpE$^{\Delta NLS2}$, Comp-MmpE$^{\Delta NLS1-2}$, Comp-MmpE-H348AN359H in THP-1 macrophages treated with or without 100 nM BEZ235; CFUs were determined at 4, 48 hpi (**C**). Data represent mean ± SD of three independent biological replicates. Statistical significance determined using two-way ANOVA, **P* < 0.05, ***P* < 0.01, ****P* < 0.001.

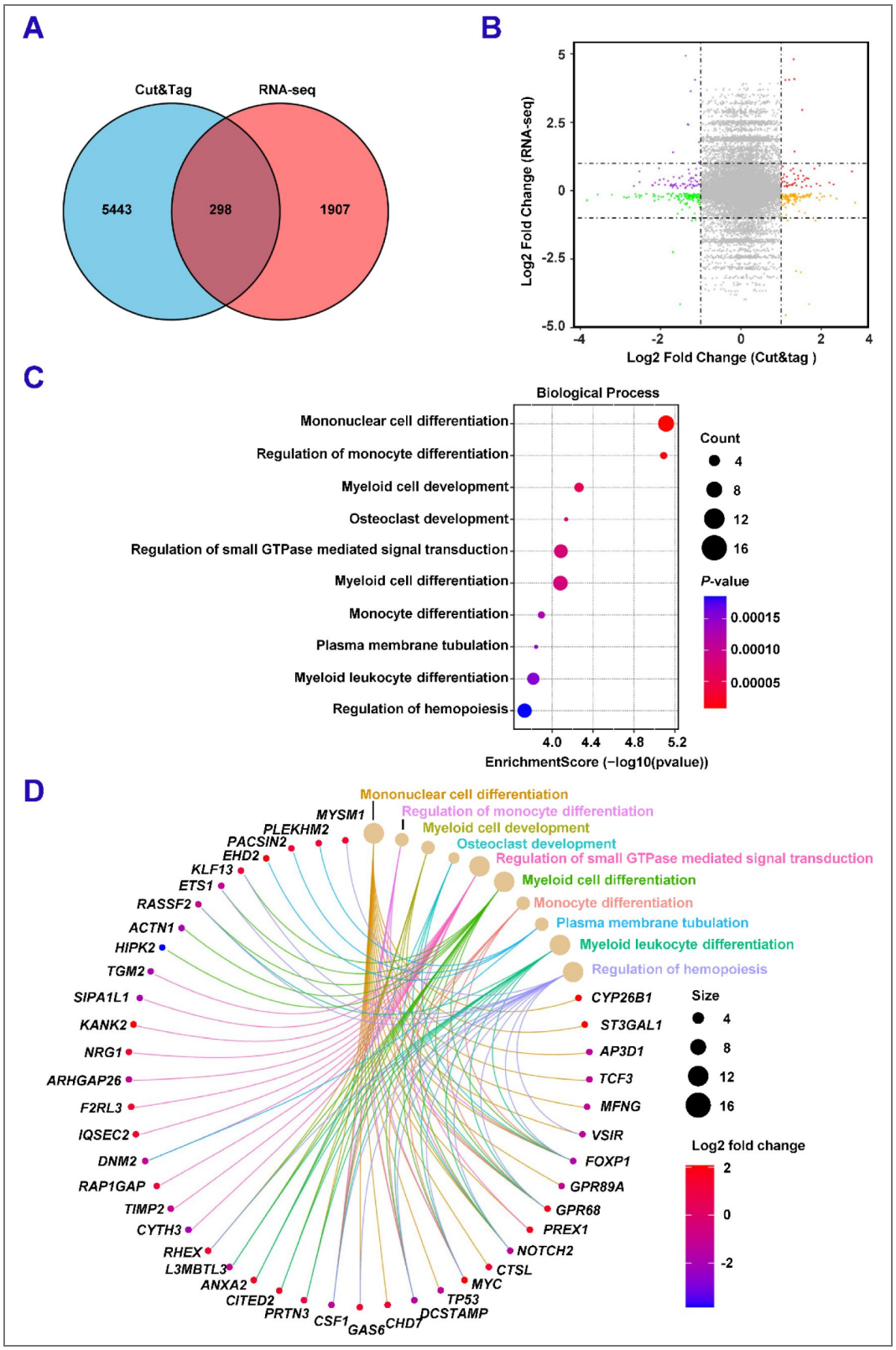

Supplementary Figure 7. MmpE modulates the transcription of immune-associated genes.

(A) Venn diagram showing the overlap between DEGs identified by RNA-seq and differential peak-associated genes identified by CUT&Tag-seq. **(B)** Four-quadrant scatter plot comparing CUT&Tag-seq and RNA-seq data. Log_2(fold change) values of peak-associated genes from CUT&Tag-seq are plotted against log_2(fold change) of FPKM values from RNA-seq. **(C)** KEGG enrichment analysis of the DEGs shown in **(A)**. **(D)** Chord diagram illustrating DEGs to enriched GO Biological Process terms.

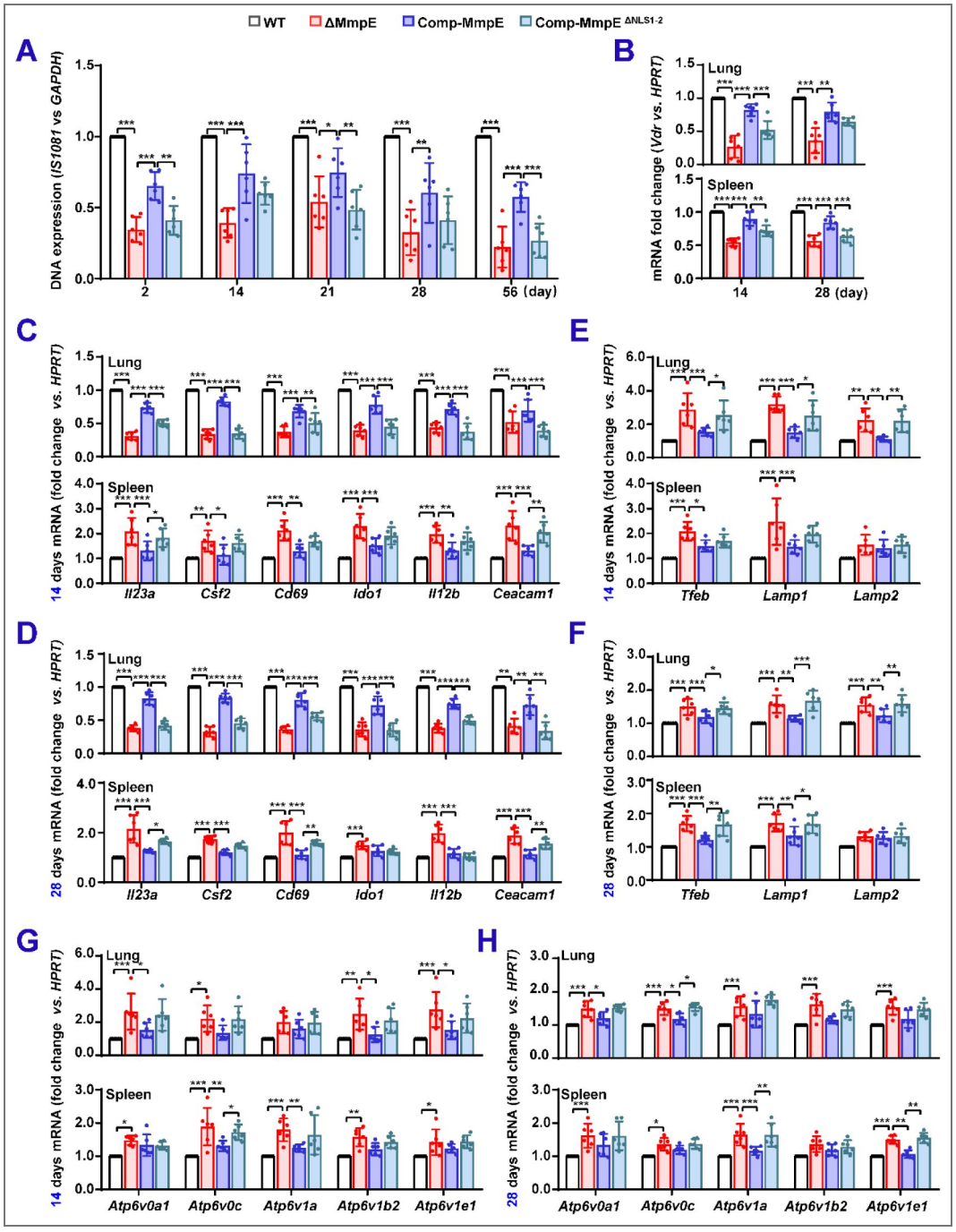

Supplementary Figure 8. MmpE facilitates bacterial colonization in the spleens of infected mice.

(A) Bacterial colonization was assessed in splenic homogenates from infected mice (as described in Figure 7A) by quantifying bacterial DNA using quantitative PCR at 2, 14, 21, 28, and 56 dpi. **(B-I)** mRNA expression in mice spleen at 14 and 28 dpi in lung and spleen tissues of infected animals. *Vdr* expression (**B**); Cytokine-related genes (**C** and **D**); lysosomal acidification (**E** and **F**) and V-ATPase subunits genes (**G** and **H**). Data represent mean ± SD of six independent biological replicates. Statistical significance determined using two-way ANOVA, **P* < 0.05, ***P* < 0.01, ****P* < 0.001.

Acknowledgements

This work was supported by the Fundamental Research Funds for the Central Universities (#2662023DKQD001), Talent Start-up Funds of Huazhong Agricultural University (#11042310008), National Natural Science Foundation of China (#32473123), China Agriculture Research System of MOF and MARA (#CARS-37), and National Key Research and Development Program of China (#2021YFD1800403).

Additional information

Author contributions

Conceptualization: L. C., A. G., and L. Z.; Methodology: L. C.; Validation: L. C., B. D., and Q. J.; Formal analysis: L. C., Y. W.; Investigation: L. C., B. D., Q. J., and Y. W.; Resources: A. G., L. Z., and Y. C.; Data curation: L. C., Q. J., and Y. W.; Writing - original draft: L. C., L. Z., and A. G.; Writing - review & editing: L. C., L. Z., and A. G.; Visualization: L. C., Q. J., Y. C., L. Z., and A. G.; Supervision: A. G., and L. Z.; Project administration: A. G., and L. Z.; Funding acquisition: A. G., L. Z., and Y. C.

Funding

Funder	Grant reference number	Author
Fundamental Research Funds for Central Universities	2662023DKQD001	Lei Zhang
Huazhong Agricultural University	11042310008	Lei Zhang
MOST | National Natural Science Foundation of China (NSFC)	32473123	Aizhen Guo
China Agriculture Research System of MOF and MARA	CARS-37	Aizhen Guo
MOST | National Key Research and Development Program of China (NKPs)	2021YFD1800403	

Author ORCID iDs

Yingyu Chen: https://orcid.org/0000-0002-1200-5314
Lei Zhang: https://orcid.org/0000-0002-8566-6068

Additional files

Table S1. Key resources used in this study.

Table S2. 175 genes were differentially expressed genes in RNA-seq.

Table S3. 2903 candidate MmpE-specific ChIP-seq signals.

Table S4. 298 genes were differentially expressed in both CUT&Tag and RNA-seq.

Table S5. Plasmids used in this study.

Table S6. Bacterial strains used in this study.

Table S7. Primers used in this study.

References

Agarwal S, Agarwal S, Jin H, Pancholi P, Pancholi V (2012) Serine/threonine phosphatase (SP-STP), secreted from Streptococcus pyogenes, is a pro-apoptotic protein. *J Biol Chem* **287**:9147-67

Aggeletopoulou I, Thomopoulos K, Mouzaki A, Triantos C (2022) Vitamin D-VDR novel anti-inflammatory molecules-new insights into their effects on liver diseases. *Int J Mol Sci* **23**:8465

Alsayed SSR, Gunosewoyo H (2024) Combating Tuberculosis via restoring the host immune capacity by targeting Mtb kinases and phosphatases. *Int J Mol Sci* **25**:12481

Baruch K, Gur-Arie L, Nadler C, Koby S, Yerushalmi G, Ben-Neriah Y, Yogev O, Shaulian E, Guttman C, Zarivach R, *et al.* (2011) Metalloprotease type III effectors that specifically cleave JNK and NF-κB. *EMBO J* **30**:221-31

Bhadouria J, Giri J (2022) Purple acid phosphatases: roles in phosphate utilization and new emerging functions. *Plant Cell Rep* **41**:33-51

Bhadouria J, Singh AP, Mehra P, Verma L, Srivastawa R, Parida SK, Giri J (2017) Identification of purple acid phosphatases in chickpea and potential roles of CaPAP7 in seed phytate accumulation. *Sci Rep* **7**:11012

Bierne H, Cossart P (2021) When bacteria target the nucleus: the emerging family of nucleomodulins. *Cell Microbiol* **14**:622-33

Buchanan G, Sargent F, Berks BC, Palmer T (2001) A genetic screen for suppressors of Escherichia coli Tat signal peptide mutations establishes a critical role for the second arginine within the twin-arginine motif. *Arch Microbiol* **177**:107-12

Cautain B, Hill R, de Pedro N, Link W (2015) >Components and regulation of nuclear transport processes. *Febs J* **282**:445-62

Chai Q, Wang L, Liu CH, Ge B (2020) New insights into the evasion of host innate immunity by Mycobacterium tuberculosis. *Cell Mol Immunol* **17**:901-913

Chandra P, Grigsby SJ, Philips JA (2022) Immune evasion and provocation by Mycobacterium tuberculosis. *Nat Rev Microbiol* **20**:750-766

Chen L, Duan B, Chen P, Jiang Q, Wang Y, Lu L, Chen Y, Hu C, Zhang L, Guo A (2025) A conserved mycobacterial nucleomodulin hijacks the host COMPASS complex to reprogram pro-inflammatory transcription and promote intracellular survival. *eLife* **14**:RP107677 https://doi.org/10.7554/eLife.107677

Chen L, Li X, Xu P, He ZG (2022) A novel zinc exporter CtpG enhances resistance to zinc toxicity and survival in *Mycobacterium bovis*. *Microbiol Spectr* **10**:e0145621

Chen Y, Du J, Zhang Z, Liu T, Shi Y, Ge X, Li YC (2014) MicroRNA-346 mediates tumor necrosis factor α-induced downregulation of gut epithelial vitamin D receptor in inflammatory bowel diseases. *Inflamm Bowel Dis* **20**:1910-8

Comba S, Menendez-Bravo S, Arabolaza A, Gramajo H (2013) Identification and physiological characterization of phosphatidic acid phosphatase enzymes involved in triacylglycerol biosynthesis in *Streptomyces coelicolor*. *Microb Cell Fact* **12**:9

Dean P, Scott JA, Knox AA, Quitard S, Watkins NJ, Kenny B (2010) The enteropathogenic *E. coli* effector EspF targets and disrupts the nucleolus by a process regulated by mitochondrial dysfunction. *PLoS Pathog* **6**:e1000961

Evans SM, Rodino KG, Adcox HE, Carlyon JA (2018) *Orientia tsutsugamushi* uses two Ank effectors to modulate NF-κB p65 nuclear transport and inhibit NF-κB transcriptional activation. *PLoS Pathog* **14**:e1007023

Fang J, Dong C, Xiong S (2022) *Mycobacterium tuberculosis* Rv0790c inhibits the cellular autophagy at its early stage and facilitates mycobacterial survival. *Front Cell Infect Microbiol* **12**:1014897

Fang S, Wan X, Zou X, Sun S, Hao X, Liang C, Zhang Z, Zhang F, Sun B, Li H, *et al.* (2021) Arsenic trioxide induces macrophage autophagy and atheroprotection by regulating ROS-dependent TFEB nuclear translocation and AKT/mTOR pathway. *Cell Death Dis* **12**:88

Feder D, McGeary RP, Mitić N, Lonhienne T, Furtado A, Schulz BL, Henry RJ, Schmidt S, Guddat LW, Schenk G (2020) Structural elements that modulate the substrate specificity of plant purple acid phosphatases: Avenues for improved phosphorus acquisition in crops. *Plant Sci* **294**:110445

Fontes MR, Teh T, Kobe B (2000) Structural basis of recognition of monopartite and bipartite nuclear localization sequences by mammalian importin-alpha. *J Mol Biol* **297**:1183-94

Forrellad MA, Blanco FC, Marrero Diaz de Villegas R, Vázquez CL, Yaneff A, García EA, Gutierrez MG, Durán R, Villarino A, Bigi F (2020) Rv2577 of *Mycobacterium tuberculosis* Is a virulence factor with dual phosphatase and phosphodiesterase functions. *Front Microbiol* **11**:570794

Ge P, Lei Z, Yu Y, Lu Z, Qiang L, Chai Q, Zhang Y, Zhao D, Li B, Pang Y, *et al.* (2022) *M. tuberculosis* PknG manipulates host autophagy flux to promote pathogen intracellular survival. *Autophagy* **18**:576-594

Gounis M, Hamidi H, Ivaska J (2025) mTORC1 shutdown unleashes TFEB to drive triple-negative breast cancer invasion. *Dev Cell* **60**:979-981

Hanford HE, Von Dwingelo J, Abu Kwaik Y (2021) Bacterial nucleomodulins: a coevolutionary adaptation to the eukaryotic command center. *PLoS Pathog* **17**:e1009184

Hodgson A, Wier EM, Fu K, Sun X, Yu H, Zheng W, Sham HP, Johnson K, Bailey S, Vallance BA, *et al.* (2015) Metalloprotease NleC suppresses host NF-κB/inflammatory responses by cleaving p65 and interfering with the p65/RPS3 interaction. *PLoS Pathog* **11**:e1004705

Hsu CM, Lin PM, Tsai YT, Tsai MS, Tseng CH, Lin SF, Yang MY (2018) NVP-BEZ235, a dual PI3K-mTOR inhibitor, suppresses the growth of FaDu hypopharyngeal squamous cell carcinoma and has a synergistic effect with Cisplatin. *Cell Death Discov* **4**:57

Jeong SJ, Stitham J, Evans TD, Zhang X, Rodriguez-Velez A, Yeh YS, Tao J, Takabatake K, Epelman S, Lodhi IJ, *et al.* (2021) Trehalose causes low-grade lysosomal stress to activate TFEB and the autophagy-lysosome biogenesis response. *Autophagy* **17**:3740-3752

Jermy A (2010) Chlamydia gets a NUE look. *Nat Rev Microbiol* **8**:614

Jose L, Ramachandran R, Bhagavat R, Gomez RL, Chandran A, Raghunandanan S, Omkumar RV, Chandra N, Mundayoor S, Kumar RA (2016) Hypothetical protein Rv3423.1 of *Mycobacterium tuberculosis* is a histone acetyltransferase. *Febs J* **283**:265-81

Kosugi S, Hasebe M, Matsumura N, Takashima H, Miyamoto-Sato E, Tomita M, Yanagawa H (2009) Six classes of nuclear localization signal specific to different binding grooves of importin alpha. *J Biol Chem* **284**:478-485

Lebreton A, Job V, Ragon M, Le Monnier A, Dessen A, Cossart P, Bierne H (2014) Structural basis for the inhibition of the chromatin repressor BAHD1 by the bacterial nucleomodulin LntA. *mBio* **5**:e00775-13

Lebreton A, Lakisic G, Job V, Fritsch L, Tham TN, Camejo A, Matteï PJ, Regnault B, Nahori MA, Cabanes D, *et al.* (2011) A bacterial protein targets the BAHD1 chromatin complex to stimulate type III interferon response. *Science* **331**:1319-21

Li T, Lu Q, Wang G, Xu H, Huang H, Cai T, Kan B, Ge J, Shao F (2013) SET-domain bacterial effectors target heterochromatin protein 1 to activate host rDNA transcription. *EMBO Rep* **14**:733-40

Li X, Chen L, Liao J, Hui J, Li W, He ZG (2020) A novel stress-inducible CmtR-ESX3- Zn^{2+} regulatory pathway essential for survival of *Mycobacterium bovis* under oxidative stress. *J Biol Chem* **295**:17083-17099

Li X, Zhang M, Zhou G, Xie Z, Wang Y, Han J, Li L, Wu Q, Zhang S (2023) Role of Rho GTPases in inflammatory bowel disease. *Cell Death Discov* **9**:24

Liu PT, Stenger S, Li H, Wenzel L, Tan BH, Krutzik SR, Ochoa MT, Schauber J, Wu K, Meinken C, *et al.* (2006) Toll-like receptor triggering of a vitamin D-mediated human antimicrobial response. *Science* **311**:1770-3

Liu SF, Yi ZC, Huang ZQ, Yuan ZD, Yang YC, Zhao Y, He QY, Yang WD, Li HY, Lin CSK, *et al.* (2025) Enhanced biodegradation of glyphosate by *Chlorella sorokiniana* engineered with exogenous purple acid phosphatase. *Water Res* **268**:122737

Ma S, Ming Y, Wu J, Cui G (2024) Cellular metabolism regulates the differentiation and function of T-cell subsets. *Cell Mol Immunol* **21**:419-435

Mitra S, Dunphy PS, Das S, Zhu B, Luo T, McBride JW (2018) *Ehrlichia chaffeensis* TRP120 effector targets and recruits host polycomb group proteins for degradation to promote intracellular infection. *Infect Immun* **86**:e00845-17

Nasiri MJ, Venketaraman V (2025) Advances in host-pathogen interactions in Tuberculosis: emerging strategies for therapeutic intervention. *Int J Mol Sci* **26**:1621

Nisa A, Kipper FC, Panigrahy D, Tiwari S, Kupz A, Subbian S (2022) Different modalities of host cell death and their impact on *Mycobacterium tuberculosis* infection. *Am J Physiol Cell Physiol* **323**:C1444-C1474

Pennini ME, Perrinet S, Dautry-Varsat A, Subtil A (2010) Histone methylation by NUE, a novel nuclear effector of the intracellular pathogen *Chlamydia trachomatis*. *PLoS Pathog* **6**:e1000995

Rodriguez F, Lillington J, Johnson S, Timmel CR, Lea SM, Berks BC (2014) Crystal structure of the *Bacillus subtilis* phosphodiesterase PhoD reveals an iron and calcium-containing active site. *J Biol Chem* **289**:30889-99

Rolando M, Sanulli S, Rusniok C, Gomez-Valero L, Bertholet C, Sahr T, Margueron R, Buchrieser C (2013) *Legionella pneumophila* effector RomA uniquely modifies host chromatin to repress gene expression and promote intracellular bacterial replication. *Cell Host Microbe* **13**:395-405

Schenk G, Guddat LW, Ge Y, Carrington LE, Hume DA, Hamilton S, de Jersey J (2000) Identification of mammalian-like purple acid phosphatases in a wide range of plants. *Gene* **250**:117-25

Sha S, Shi Y, Tang Y, Jia L, Han X, Liu Y, Li X, Ma Y (2021) *Mycobacterium tuberculosis* Rv1987 protein induces M2 polarization of macrophages through activating the PI3K/Akt1/mTOR signaling pathway. *Immunol Cell Biol* **99**:570-585

Shaban L, Nguyen GT, Mecsas-Faxon BD, Swanson KD, Tan S, Mecsas J (2020) *Yersinia pseudotuberculosis* YopH targets SKAP2-dependent and independent signaling pathways to block neutrophil antimicrobial mechanisms during infection. *PLoS Pathog* **16**:e1008576

Singh AP, Sharma S, Pagarware K, Siraji RA, Ansari I, Mandal A, Walling P, Aijaz S (2018) Enteropathogenic *E. coli* effectors EspF and Map independently disrupt tight junctions through distinct mechanisms involving transcriptional and post-transcriptional regulation. *Sci Rep* **8**:3719

Singh PR, Dadireddy V, Udupa S, Kalladi SM, Shee S, Khosla S, Rajmani RS, Singh A, Ramakumar S, Nagaraja V (2023) The *Mycobacterium tuberculosis* methyltransferase Rv2067c manipulates host epigenetic programming to promote its own survival. *Nat Commun* **14**:8497

Singh PR, Nagaraja V (2025) Epigenetic maneuvering: an emerging strategy for mycobacterial intracellular survival. *Trends Microbiol* **33**:354-369

Stanley NR, Palmer T, Berks BC (2000) The twin arginine consensus motif of Tat signal peptides is involved in Sec-independent protein targeting in *Escherichia coli*. *J Biol Chem* **275**:11591-6

Steiert B, Weber MM (2025) Nuclear warfare: pathogen manipulation of the nuclear pore complex and nuclear functions. *mBio* **16**:e0194024

Tang D, Chen M, Huang X, Zhang G, Zeng L, Zhang G, Wu S, Wang Y (2023) SRplot: A free online platform for data visualization and graphing. *PLoS One* **18**:e0294236

Tian J, Zhu Y, Rao M, Cai Y, Lu Z, Zou D, Peng X, Ying P, Zhang M, Niu S, *et al.* (2020) N^6-methyladenosine mRNA methylation of PIK3CB regulates AKT signalling to promote PTEN-deficient pancreatic cancer progression. *Gut* **69**:2180-2192

Usategui-Martín R, De Luis-Román DA, Fernández-Gómez JM, Ruiz-Mambrilla M, Pérez-Castrillón JL (2022) Vitamin D receptor (VDR) gene polymorphisms modify the response to vitamin d supplementation: a systematic review and meta-analysis. *Nutrients* **14**:360

Wang B, Martini-Stoica H, Qi C, Lu TC, Wang S, Xiong W, Qi Y, Xu Y, Sardiello M, Li H, *et al.* (2024) TFEB-vacuolar ATPase signaling regulates lysosomal function and microglial activation in tauopathy. *Nat Neurosci* **27**:48-62

Wang J, Ge P, Qiang L, Tian F, Zhao D, Chai Q, Zhu M, Zhou R, Meng G, Iwakura Y, *et al.* (2017) The mycobacterial phosphatase PtpA regulates the expression of host genes and promotes cell proliferation. *Nat Commun* **8**:244

Wong D, Bach H, Sun J, Hmama Z, Av-Gay Y (2011) *Mycobacterium tuberculosis* protein tyrosine phosphatase (PtpA) excludes host vacuolar-H^+-ATPase to inhibit phagosome acidification. *Proc Natl Acad Sci U S A* **108**:19371-6

Yang H, Zhang H, Li Y, Xiang L, Liu J (2019) BCG stimulation promotes dendritic cell proliferation and expression of VDR and CYP27B1 in vitamin D-deficient mice. *Mol Med Rep* **20**:5265-5271

Yang L, Shi P, Zhao G, Xu J, Peng W, Zhang J, Zhang G, Wang X, Dong Z, Chen F, *et al.* (2020) Targeting cancer stem cell pathways for cancer therapy. *Signal Transduct Target Ther* **5**:8

Yeung SL, Cheng C, Lui TK, Tsang JS, Chan WT, Lim BL (2009) Purple acid phosphatase-like sequences in prokaryotic genomes and the characterization of an atypical purple alkaline phosphatase from *Burkholderia cenocepacia* J2315. *Gene* **440**:1-8

Zhang L, Kent JE, Whitaker M, Young DC, Herrmann D, Aleshin AE, Ko YH, Cingolani G, Saad JS, Moody DB, *et al.* (2022) A periplasmic cinched protein is required for siderophore secretion and virulence of *Mycobacterium tuberculosis*. *Nat Commun* **13**:2255

Zhang QA, Ma S, Li P, Xie J (2023) The dynamics of *Mycobacterium tuberculosis* phagosome and the fate of infection. *Cell Signal* **108**:110715

Zhang W, Dong C, Xiong S (2024) Mycobacterial SapM hampers host autophagy initiation for intracellular bacillary survival via dephosphorylating Raptor. *iScience* **27**:109671

Zheng R, Li Z, Fang W, Lou H, Liu F, Sun Q, Shi X, Liu H, Chen Q, Shen X, *et al.* (2025) A genome-wide association study identified PRKCB as a causal gene and therapeutic target for Mycobacterium avium complex disease. *Cell Rep Med* **6**:101923

Zhou Y, Dong B, Kim KH, Choi S, Sun Z, Wu N, Wu Y, Scott J, Moore DD (2020) Vitamin D Receptor Activation in Liver Macrophages Protects Against Hepatic Endoplasmic Reticulum Stress in Mice. *Hepatology* **71**:1453-1466

Peer reviews

Reviewer #1 (Public review):

Summary:

The study provides insightful characterization of the mycobacterial secreted effector protein MmpE which translocates to the host nucleus and exhibits phosphatase activity. The study characterizes the nuclear localization signal sequences and residues critical for the phosphatase activity, both of which are required for intracellular survival

Strengths:

(1) The study addresses the role of nucleomodulins, an understudied aspect in mycobacterial infections.

(2) The authors employ a combination of biochemical and computational analyses along with in vitro and in vivo validations to characterize the role of MmpE.

Weaknesses:

(1) While the study establishes that the phosphatase activity of MmpE operates independently of its NLS, there is a clear gap in understanding how this phosphatase activity supports mycobacterial infection. The investigation lacks experimental data on specific substrates of MmpE or pathways influenced by this virulence factor.

(2) The study does not explore whether the phosphatase activity of MmpE is dependent on the NLS within macrophages, which would provide critical insights into its biological relevance in host cells. Conducting experiments with double knockout/mutant strains and comparing their intracellular survival with single mutants could elucidate these dependencies and further validate the significance of MmpE's dual functions.

(3) The study does not provide direct experimental validation of the MmpE deletion on lysosomal trafficking of the bacteria.

(4) The role of MmpE as a mycobacterial effector would be more relevant using virulent mycobacterial strains such as H37Rv.

Comments on revisions:

I appreciate the work the authors have done to address reviewers comments. The revised manuscript looks significantly improved. My major concern in the revised version is the microscopy data where the BCG staining using the DiD fluorescent stain does not bring out the rod-shaped bacilli structure. I suggest the authors either use a GFP reporter or some other fluorescent stain to address this issue.

https://doi.org/10.7554/eLife.108037.2.sa3

Reviewer #2 (Public review):

Summary:

In this paper, the authors have characterized Rv2577 as a Fe3+/Zn2+ -dependent metallophosphatase and a nucleomodulin protein. The authors have also identified His348 and Asn359 as critical residues for Fe3+ coordination. The authors show that the proteins encode for two nuclease localization signals. Using C-terminal Flag expression constructs, the authors have shown that MmpE protein is secretory. The authors have prepared genetic deletion strains and show that MmpE is essential for intracellular survival of M. bovis BCG in THP-1 macrophages, RAW264.7 macrophages and mice model of infection. The authors have also performed RNA-seq analysis to compare the transcriptional profiles of macrophages infected with wild type and mmpE mutant strain. The relative levels of ~ 175 transcripts were altered in mmpE mutant infected macrophages and majority of these were associated with various immune and inflammatory signalling pathways. Using these deletion strains, the authors proposed that MmpE inhibits inflammatory gene expression by binding to the promoter region of vitamin D receptor. The authors also showed that MmpE arrests phagosome maturation by regulating the expression of several lysosome associated genes such as TFEB, LAMP1, LAMP2 etc. These findings reveal a sophisticated mechanism by which a bacterial effector protein manipulates gene transcription and promotes intracellular survival.

Strength:

The authors have used a combination of cell biology, microbiology and transcriptomics to elucidate the mechanisms by which Rv2577 contributes to intracellular survival.

Weakness:

The authors should thoroughly check the mice data and show individual replicate values in bar graphs.

Comments on revisions:

Thanks to the authors for addressing the concerns raised during the review of the original manuscript. The data is now presented with clarity, and discrepancies in mouse experiments have also been addressed with additional experiments.

https://doi.org/10.7554/eLife.108037.2.sa2

Reviewer #3 (Public review):

Summary:

In this manuscript titled "Mycobacterial Metallophosphatase MmpE Acts as a Nucleomodulin to Regulate Host Gene Expression and Promote Intracellular Survival", Chen et al describe biochemical characterisation, localisation and potential functions of the gene using a genetic approach in M. bovis BCG and perform macrophage and mice infections to understand the roles of this potentially secreted protein in the host cell nucleus. The findings demonstrate the role of a secreted phosphatase of M. bovis BCG in shaping the transcriptional profile of infected macrophages, potentially through nuclear localisation and direct binding to transcriptional start sites, thereby regulating the inflammatory response to infection.

Strengths:

The authors demonstrate using a transient transfection method that MmpE when expressed as a GFP-tagged protein in HEK293T cells, exhibits nuclear localisation. The authors identify two NLS motifs that together are required for nuclear localisation of the protein. A deletion of the gene in M. bovis BCG results in poorer survival compared to the wild type parent strain, which is also killed by macrophages. Relative to the WT strain infected macrophages, macrophages infected with the mmpE strain exhibited differential gene expression. Overexpression of the gene in HEK293T led to occupancy of the transcription start site of several genes, including the Vitamin D Receptor. Expression of VDR in THP1 macrophages was lower in case of mmpE infection compared to WT infection. This data supports the utility of the overexpression system in identifying potential target loci of MmpE using the HEK293T transfection model. The authors also demonstrate that the protein is a phosphatase and the phosphatase activity of the protein is partially required for bacterial survival but not for regulation of the VDR gene expression.

Weaknesses:

There are significant differences in lysosomal retention between M. tuberculosis and M. bovis BCG. This study uses BCG and MMPE overexpression to draw conclusions about the impact of the MMPE gene on host gene expression and the bacteria's lysosomal localisation. While the authors have convincingly supported their claims with this model system, the relevance of this mechanism in M. tuberculosis infection remains unaddressed.

https://doi.org/10.7554/eLife.108037.2.sa1

Author response:

The following is the authors' response to the original reviews.

> ***Public Reviews:***
>
> ***Reviewer #1 (Public review):***
>
> *Summary:*

> *Review of the manuscript titled " Mycobacterial Metallophosphatase MmpE acts as a nucleomodulin to regulate host gene expression and promotes intracellular survival".*
>
> *The study provides an insightful characterization of the mycobacterial secreted effector protein MmpE, which translocates to the host nucleus and exhibits phosphatase activity. The study characterizes the nuclear localization signal sequences and residues critical for the phosphatase activity, both of which are required for intracellular survival.*
>
> *Strengths:*
>
> *(1) The study addresses the role of nucleomodulins, an understudied aspect in mycobacterial infections.*
>
> *(2) The authors employ a combination of biochemical and computational analyses along with in vitro and in vivo validations to characterize the role of MmpE.*
>
> *Weaknesses:*
>
> *(1) While the study establishes that the phosphatase activity of MmpE operates independently of its NLS, there is a clear gap in understanding how this phosphatase activity supports mycobacterial infection. The investigation lacks experimental data on specific substrates of MmpE or pathways influenced by this virulence factor.*

We thank the reviewer for this insightful comment and agree that identification of the substrates of MmpE is important to fully understand its role in mycobacterial infection. MmpE is a putative purple acid phosphatase (PAP) and a member of the metallophosphoesterase (MPE) superfamily. Enzymes in this family are known for their catalytic promiscuity and broad substrate specificity, acting on phosphomonoesters, phosphodiesters, and phosphotriesters (Matange et al., Biochem J, 2015). In bacteria, several characterized MPEs have been shown to hydrolyze substrates such as cyclic nucleotides (e.g., cAMP) (Keppetipola et al., J Biol Chem, 2008; Shenoy et al., J Mol Biol, 2007), nucleotide derivatives (e.g., AMP, UDP-glucose) (Innokentev et al., mBio, 2025), and pyrophosphate-containing compounds (e.g., Ap4A, UDP-DAGn) (Matange et al., Biochem J., 2015). Although the binding motif of MmpE has been identified, determining its physiological substrates remains challenging due to the low abundance and instability of potential metabolites, as well as the limited sensitivity and coverage of current metabolomic technologies in mycobacteria.

> *(2) The study does not explore whether the phosphatase activity of MmpE is dependent on the NLS within macrophages, which would provide critical insights into its biological relevance in host cells. Conducting experiments with double knockout/mutant strains and comparing their intracellular survival with single mutants could elucidate these dependencies and further validate the significance of MmpE's dual functions.*

We thank the reviewer for the comment. Deletion of the NLS motifs did not impair MmpE's phosphatase activity in vitro (Figure 2F), indicating that MmpE's enzymatic function operates independently of its nuclear localization. Indeed, we confirmed that Fe^{3+}-binding ability via the residues H348 and N359 is required for enzymatic activity of MmpE. We have expanded on this point in the Discussion section "MmpE is a bifunctional virulence factor in Mtb".

> *(3) The study does not provide direct experimental validation of the MmpE deletion on lysosomal trafficking of the bacteria.*

We thank the reviewer for the comment. To validate the role of MmpE in lysosome maturation during infection, we conducted fluorescence colocalization assays in THP-1 macrophages infected with BCG strains, including WT, ΔMmpE, Comp-MmpE, Comp-$MmpE^{\Delta NLS1}$, Comp-$MmpE^{\Delta NLS2}$, Comp-$MmpE^{\Delta NLS1\text{-}2}$. These strains were stained with the

lipophilic membrane dye DiD, while macrophages were treated with the acidotropic probe LysoTracker^{TM} Green (Martins et al., Autophagy, 2019). The result indicated that ΔMmpE and MmpE^{NLS1-2} mutants exhibited significantly higher co-localization with LysoTracker compared to WT and Comp-MmpE strains (New Figure 5G), suggesting that MmpE deletion leads to enhanced lysosomal maturation during infection.

> *(4) The role of MmpE as a mycobacterial effector would be more relevant using virulent mycobacterial strains such as H37Rv.*

We thank the reviewer for the comment. Previously, the role of Rv2577/MmpE as a virulence factor has been demonstrated in *M. tuberculosis* CDC 1551, where its deletion significantly reduced bacterial replication in mouse lungs at 30 days post-infection (Forrellad et al., Front Microbiol, 2020). However, that study did not explore the underlying mechanism of MmpE function. In our study, we found that MmpE enhances *M. bovis* BCG survival in macrophages (THP-1 and RAW264.7 both) and in mice (Figure 3, Figure 7A), consistent with its proposed role in virulence. To investigate the molecular mechanism by which MmpE promotes intracellular survival, we used *M. bovis* BCG as a biosafe surrogate and this model is widely accepted for studying mycobacterial pathogenesis (Wang et al., Nat Immunol, 2015; Wang et al., Nat Commun, 2017; Péan et al., Nat Commun, 2017).

> ***Reviewer #2 (Public review):***
>
> *Summary:*
>
> *In this paper, the authors have characterized Rv2577 as a Fe3+/Zn2+ -dependent metallophosphatase and a nucleomodulin protein. The authors have also identified His348 and Asn359 as critical residues for Fe3+ coordination. The authors show that the proteins encode for two nuclease localization signals. Using C-terminal Flag expression constructs, the authors have shown that the MmpE protein is secretory. The authors have prepared genetic deletion strains and show that MmpE is essential for intracellular survival of M. bovis BCG in THP-1 macrophages, RAW264.7 macrophages, and a mouse model of infection. The authors have also performed RNA-seq analysis to compare the transcriptional profiles of macrophages infected with wild-type and MmpE mutant strains. The relative levels of ~ 175 transcripts were altered in MmpE mutant-infected macrophages and the majority of these were associated with various immune and inflammatory signalling pathways. Using these deletion strains, the authors proposed that MmpE inhibits inflammatory gene expression by binding to the promoter region of a vitamin D receptor. The authors also showed that MmpE arrests phagosome maturation by regulating the expression of several lysosome-associated genes such as TFEB, LAMP1, LAMP2, etc. These findings reveal a sophisticated mechanism by which a bacterial effector protein manipulates gene transcription and promotes intracellular survival.*
>
> *Strength:*
>
> *The authors have used a combination of cell biology, microbiology, and transcriptomics to elucidate the mechanisms by which Rv2577 contributes to intracellular survival.*
>
> *Weakness:*
>
> *The authors should thoroughly check the mice data and show individual replicate values in bar graphs.*

We kindly appreciate the reviewer for the advice. We have now updated the relevant mice data in the revised manuscript.

> ***Reviewer #3 (Public review):***
>
> *Summary:*

> *In this manuscript titled "Mycobacterial Metallophosphatase MmpE Acts as a Nucleomodulin to Regulate Host Gene Expression and Promote Intracellular Survival", Chen et al describe biochemical characterisation, localisation and potential functions of the gene using a genetic approach in M. bovis BCG and perform macrophage and mice infections to understand the roles of this potentially secreted protein in the host cell nucleus. The findings demonstrate the role of a secreted phosphatase of M. bovis BCG in shaping the transcriptional profile of infected macrophages, potentially through nuclear localisation and direct binding to transcriptional start sites, thereby regulating the inflammatory response to infection.*
>
> *Strengths:*
>
> *The authors demonstrate using a transient transfection method that MmpE when expressed as a GFP-tagged protein in HEK293T cells, exhibits nuclear localisation. The authors identify two NLS motifs that together are required for nuclear localisation of the protein. A deletion of the gene in M. bovis BCG results in poorer survival compared to the wild-type parent strain, which is also killed by macrophages. Relative to the WT strain-infected macrophages, macrophages infected with the ΔmmpE strain exhibited differential gene expression. Overexpression of the gene in HEK293T led to occupancy of the transcription start site of several genes, including the Vitamin D Receptor. Expression of VDR in THP1 macrophages was lower in the case of ΔmmpE infection compared to WT infection. This data supports the utility of the overexpression system in identifying potential target loci of MmpE using the HEK293T transfection model. The authors also demonstrate that the protein is a phosphatase, and the phosphatase activity of the protein is partially required for bacterial survival but not for the regulation of the VDR gene expression.*
>
> *Weaknesses:*
>
> *(1) While the motifs can most certainly behave as NLSs, the overexpression of a mycobacterial protein in HEK293T cells can also result in artefacts of nuclear localisation. This is not unprecedented. Therefore, to prove that the protein is indeed secreted from BCG, and is able to elicit transcriptional changes during infection, I recommend that the authors (i) establish that the protein is indeed secreted into the host cell nucleus, and (ii) the NLS mutation prevents its localisation to the nucleus without disrupting its secretion.*

We kindly appreciate the reviewer for this insightful comment. To confirm the translocation of MmpE into the host nucleus during BCG infection, we first detected the secretion of MmpE by *M. bovis* BCG, using Ag85B as a positive control and GlpX as a negative control (Zhang et al., Nat commun, 2022). Our results showed that MmpE- Flag was present in the culture supernatant, indicating that MmpE is secreted by BCG indeed (new Figure S1C).

Next, we performed immunoblot analysis of the nuclear fractions from infected THP-1 macrophages expressing FLAG-tagged wild-type MmpE and NLS mutants. The results revealed that only wild-type MmpE was detected in the nucleus, while $MmpE^{\Delta NLS1}$, $MmpE^{\Delta NLS2}$ and $MmpE^{\Delta NLS1\text{-}2}$ were not detectable in the nucleus (New Figure S1D). Taken together, these findings demonstrated that MmpE is a secreted protein and that its nuclear translocation during infection requires both NLS motifs.

> *Demonstration that the protein is secreted: Supplementary Figure 3 - Immunoblotting should be performed for a cytosolic protein, also to rule out detection of proteins from lysis of dead cells. Also, for detecting proteins in the secreted fraction, it would be better to use Sauton's media without detergent, and grow the cultures without agitation or with gentle agitation. The method used by the authors is not a recommended protocol for obtaining the secreted fraction of mycobacteria.*

We kindly appreciate the reviewer for the advice. To avoid the effects of bacterial lysis, we cultured the BCG strains expressing MmpE-Flag in Middlebrook 7H9 broth with 0.5% glycerol, 0.02% Tyloxapol, and 50 μg/mL kanamycin at 37 °C with gentle agitation (80 rpm) until an OD_{600} of approximately 0.6 (Zhang et al., Nat Commun, 2022). Subsequently, we assessed the secretion of MmpE-Flag in the culture supernatant, using Ag85B as a positive control and GlpX as a negative control (New Figure S1C). The results showed that GlpX was not detected in the supernatant, while MmpE and Ag85B were detected, indicating that MmpE is indeed a secreted protein in BCG.

> *Demonstration that the protein localises to the host cell nucleus upon infection: Perform an infection followed by immunofluorescence to demonstrate that the endogenous protein of BCG can translocate to the host cell nucleus. This should be done for an NLS1-2 mutant expressing cell also.*

We thank the reviewer for the suggestion. We agree that this experiment would be helpful to further verify the ability of MmpE for nuclear import. However, MmpE specific antibody is not available for us for immunofluorescence experiment. Alternatively, we performed nuclear-cytoplasmic fractionation for the THP-1 cells infected with the *M. bovis* BCG strains expressing FLAG-tagged wild-type MmpE, as well as NLS deletion mutants ($MmpE^{\Delta NLS1}$, $MmpE^{\Delta NLS2}$, and $MmpE^{\Delta NLS1\text{-}2}$). The WT MmpE is detectable in both cytoplasmic and nuclear compartments, while $MmpE^{\Delta NLS1}$, $MmpE^{\Delta NLS2}$ or $MmpE^{\Delta NLS1\text{-}2}$ were almost undetectable in nuclear fractions (New Figure S1D), suggesting that both NLS motifs are necessary for nuclear import.

> *(2) In the RNA-seq analysis, the directionality of change of each of the reported pathways is not apparent in the way the data have been presented. For example, are genes in the cytokine-cytokine receptor interaction or TNF signalling pathway expressed more, or less in the ΔmmpE strain?*

We thank the reviewer for the comment. The KEGG pathway enrichment diagrams in our RNA-seq analysis primarily reflect the statistical significance of pathway enrichment based on differentially expressed genes, but do not indicate the directionality of genes expression changes. To address this concern, we conducted qRT-PCR on genes associated with the cytokine-cytokine receptor interaction pathway, specifically *IL23A*, *CSF2*, and *IL12B*. The results showed that, compared to the WT strain, infection with the ΔMmpE strain resulted in significantly increased expression levels of these genes in THP-1 cells (Figure 4F, Figure S4B), consistent with the RNA-seq data. Furthermore, we have submitted the complete RNA-seq dataset to the NCBI GEO repository [GSE312039], which includes normalized expression values and differential expression results for all detected genes.

> *(3) Several of these pathways are affected as a result of infection, while others are not induced by BCG infection. For example, BCG infection does not, on its own, produce changes in IL1β levels. As the author s did not compare the uninfected macrophages as a control, it is difficult to interpret whether ΔmmpE induced higher expression than the WT strain, or simply did not induce a gene while the WT strain suppressed expression of a gene. This is particularly important because the strain is attenuated. Does the attenuation have anything to do with the ability of the protein to induce lysosomal pathway genes? Does induction of this pathway lead to attenuation of the strain? Similarly, for pathways that seem to be downregulated in the ΔmmpE strain compared to the WT strain, these might have been induced upon infection with the WT strain but not sufficiently by the ΔmmpE strain due to its attenuation/ lower bacterial burden.*

We thank the reviewer for the comment. Previous studies have shown that wild-type BCG induces relatively low levels of IL-1β, while retaining partial capacity to activate the inflammasome (Qu et al., Sci Adv, 2020). Our data (Figures 3G) show that infection with the

ΔMmpE strain results in enhanced IL-1β expression, consistent with findings by Master et al. (Cell Host Microbe, 2008), in which deletion of *zmp1* in BCG or *M. tuberculosis* led to increased IL-1β levels due to reduced inhibition of inflammasome activation.

In the revised manuscript, we have provided additional qRT-PCR data using uninfected macrophages as a baseline control. These results demonstrate that the WT strain suppresses lysosome-associated gene expression, whereas the ΔMmpE strain upregulates these genes, indicating that MmpE inhibits lysosome-related genes expression (Figure 4G). Furthermore, bacterial burden analysis revealed that Δ*mmpE* exhibited ~3-fold lower intracellular survival than the WT strain in THP-1 cells. However, when lysosomal maturation was inhibited, the difference in bacterial load between the two strains was reduced to ~1-fold (New Figures S6B and C). These findings indicate that MmpE promotes intracellular survival primarily by inhibiting lysosomal maturation, which is consistent with a previous study (Chandra et al., Sci Rep, 2015).

> *(4) CHIP-seq should be performed in THP1 macrophages, and not in HEK293T. Overexpression of a nuclear-localised protein in a non-relevant line is likely to lead to several transcriptional changes that do not inform us of the role of the gene as a transcriptional regulator during infection.*

We thank the reviewer for the comment. We performed ChIP-seq in HEK293T cells based on their high transfection efficiency, robust nuclear protein expression, and well-annotated genome (Lampe et al., Nat Biotechnol, 2024; Marasco et al., Cell, 2022). These characteristics make HEK293T an ideal system for the initial identification of genome-wide chromatin binding profiles by MmpE.

Further, we performed comprehensive validation of the ChIP-seq findings in THP-1 macrophages. First, CUT&Tag and RNA-seq analyses in THP-1 cells revealed that MmpE modulates genes involved in the PI3K–AKT signaling and lysosomal maturation pathways (Figure 4C; Figure S5A-B). Correspondingly, we found that infection with the ΔMmpE strain led to reduced phosphorylation of AKT (S473), mTOR (S2448), and p70S6K (T389) (New Figure 5E-F), and upregulation of lysosomal genes such as TFEB, LAMP1, and LAMP2 (Figure 4G), compared to infection with the WT strain, and lysosomal maturation in cells infected with the ΔMmpE strain more obviously (New Figure 5G). Additionally, CUT&Tag profiling identified MmpE binding at the promoter region of the *VDR* gene, which was further validated by EMSA and ChIP-qPCR. Also, qRT-PCR demonstrated that MmpE suppresses VDR transcription, supporting its role as a transcriptional regulator (Figure 6). Collectively, these data confirm the biological relevance and functional significance of the ChIP-seq findings obtained in HEK293T cells.

> *(5) I would not expect to see such large inflammatory reactions persisting 56 days post-infection with M. bovis BCG. Is this something peculiar for an intratracheal infection with 1x107 bacilli? For images of animal tissue, the authors should provide images of the entire lung lobe with the zoomed-in image indicated as an inset.*

We thank the reviewer for the comment. The lung inflammation peaked at days 21–28 and had clearly subsided by day 56 across all groups (New Figure 7B), consistent with the expected resolution of immune responses to an attenuated strain like *M. bovis* BCG. This temporal pattern is in line with previous studies using intravenous or intratracheal BCG vaccination in mice and macaques, which also demonstrated robust early immune activation followed by resolution over time (Smith et al., Nat Microbiol, 2025; Darrah et al., Nature, 2020).

In this study, the infectious dose (1×10^7 CFU intratracheal) was selected based on previous studies in which intratracheal delivery of 1×10^7 CFU produced consistent and measurable lung immune responses and pathology without causing overt illness or mortality (Xu et al.,

Sci Rep, 2017; Niroula et al., Sci Rep, 2025). We have provided whole-lung lobe images with zoomed-in insets in the source dataset.

> *(6) For the qRT-PCR based validation, infections should be performed with the MmpE-complemented strain in the same experiments as those for the WT and ΔmmpE strain so that they can be on the same graph, in the main manuscript file. Supplementary Figure 4 has three complementary strains. Again, the absence of the uninfected, WT, and ΔmmpE infected condition makes interpretation of these data very difficult.*

We thank the reviewer for the comment. As suggested, we have conducted the qRT-PCR experiment including the uninfected, WT, ΔmmpE, Comp-MmpE, and the three complementary strains infecting THP-1 cells (Figure 4F and G; New Figure S4B–D).

> *(7) The abstract mentions that MmpE represses the PI3K-Akt-mTOR pathway, which arrests phagosome maturation. There is not enough data in this manuscript in support of this claim. Supplementary Figure 5 does provide qRT-PCR validation of genes of this pathway, but the data do not indicate that higher expression of these pathways, whether by VDR repression or otherwise, is driving the growth restriction of the ΔmmpE strain.*

We thank the reviewer for the comment. In the updated manuscript, we have provided more evidence. First, the RNA-seq analysis indicated that MmpE affects the PI3K-AKT signaling pathway (Figure 4C). Second, CUT&Tag analysis suggested that MmpE binds to the promoter regions of key pathway components, including *PRKCB*, *PLCG2*, and *PIK3CB* (Figure S5A). Third, confocal microscopy showed that ΔMmpE strain promotes significantly increased lysosomal maturation compared to the WT, a process downstream of the PI3K-AKT-mTOR axis (New Figure 5G).

Further, we measured protein phosphorylation for validating activation of the pathway (Zhang et al., Stem Cell Reports, 2017). Our results showed that cells infected with WT strains exhibited significantly higher phosphorylation of Akt, mTOR, and p70S6K compared to those infected with ΔMmpE strains (New Figures 5E and F). Moreover, the dual PI3K/mTOR inhibitor BEZ235 abolished the survival advantage of WT strains over ΔMmpE mutants in THP-1 macrophages (New Figure S6B and C). Collectively, these results support that MmpE activates the PI3K–Akt–mTOR signaling pathway to enhance bacterial survival within the host.

> *(8) The relevance of the NLS and the phosphatase activity is not completely clear in the CFU assays and in the gene expression data. Firstly, there needs to be immunoblot data provided for the expression and secretion of the NLS-deficient and phosphatase mutants. Secondly, CFU data in Figure 3A, C, and E must consistently include both the WT and ΔmmpE strain.*

We thank the reviewer for the comment. We have now added immunoblot analysis for expression and secretion of MmpE mutants. The result show that NLS-deficient and phosphatase mutants can detected in supernatant (New Figure S1C). Additionally, we have revised Figures 3A, 3C, and 3E to consistently include both the WT and ΔMmpE strains in the CFU assays (Figures 3A, 3C, and 3E).

> ***Recommendations for the authors:***
>
> ***Reviewer #2 (Recommendations for the authors):***
>
> *The authors should attempt to address the following comments:*
>
> *(1) Please perform densitometric analysis for the western blot shown in Figure 1E.*

We sincerely thank the reviewer for the suggestion. In the updated manuscript, we have performed densitometric analysis of the western blot shown in New Figure 1F and G.

> *(2) Is it possible to measure the protein levels for MmpE in lysates prepared from infected macrophages.*

We thank the reviewer for the comment. In the revised manuscript, we performed immunoblot analysis to measure MmpE levels in lysates from infected macrophages. The results demonstrated that wild-type MmpE was present in both the cytoplasmic and nuclear fractions during infection in THP-1 cells (New Figure S1D).

> *(3) The authors should perform circular dichroism studies to compare the secondary structure of wild type and mutant proteins (in particular MmpEHis348 and MmpEAsn359.*

We thank the reviewer for this valuable suggestion. We agree that circular dichroism spectroscopy could provide useful information in comparison of the differences on the secondary structures. However, due to the technical limitations, we instead compared the structures of wild-type MmpE and the His348 and Asn359 mutant proteins predicted by AlphaFold. These structural models showed almost no differences in secondary structures between the wild-type and mutants (Figure S1B).

> *(4) The authors should perform more experiments to determine the binding motif for MmpE in the promoter region of VDR.*

We thank the reviewer for this suggestion. In the current study, we have identified the MmpE-binding motif within the promoter region of VDR using CUT&Tag sequencing. This prediction was further validated by ChIP-qPCR and EMSA (Figure 6). These complementary approaches collectively support the identification of a specific MmpE-binding motif and demonstrate its functional relevance. Such approach was acceptable in many publications (Wen et al., Commun Biol, 2020; Li et al., Nat Commun, 2022).

> *(5) Were the transcript levels of VDR also measured in the lung tissues of infected animals?*

We thank the reviewer for this suggestion. In the revised manuscript, we have performed qRT-PCR to assess VDR transcript levels in the lung tissues of infected mice (New Figure S8B).

> *(6) How does MmpE regulate the expression of lysosome-associated genes?*

We thank the reviewer for this question. Our experiments suggested that MmpE suppresses lysosomal maturation probably by activating the host PI3K–AKT–mTOR signaling pathway (New Figure 5E–I). This pathway is well established as a negative regulator of lysosome biogenesis and function (Yang et al., Signal Transduct Target Ther, 2020; Cui et al., Nature, 2023; Cui et al., Nature, 2025). During infection, THP-1 cells infected with the WT showed increased phosphorylation of Akt, mTOR, and p70S6K compared to those infected with ΔMmpE (New Figure S5C, New Figure 5E and F), and concurrently downregulated key lysosomal maturation markers, including TFEB, LAMP1, LAMP2, and multiple V-ATPase subunits (Figure 4G). Given that PI3K–AKT–mTOR signaling suppresses TFEB activity and lysosomal gene transcription (Palmieri et al., Nat Commun, 2017), we propose that MmpE modulates lysosome-associated gene expression and lysosomal function probably by PI3K–AKT–mTOR signaling pathway.

> *(7) Mice experiment:*
>
> *(a) The methods section states that mice were infected intranasally, but the legend for Figure 6 states intratracheally. Kindly check?*
>
> *(b) Supplementary Figure 7 - this is not clear. The legend says bacterial loads in spleens (CFU/g) instead of DNA expression, as shown in the figure.*

> *(c) The data in Figure 6 and Figure S7 seem to be derived from the same experiment, but the number of animals is different. In Figure 6, it is n = 6, and in Figure S7, it is n=3.*

We thank the reviewer for the comments.

(a) The infection was performed intranasally, and the figure legend for New Figure 7 has now been corrected.

(b) We adopted quantitative PCR method to measure bacterial DNA levels in the spleens of infected mice. We have now revised the legend.

(c) We have conducted new experiments where each experiment now includes six mice. The results are showed in Figure 7B and C, as well as in the new Figure S8.

> *(8) The authors should show individual values for various replicates in bar graphs (for all figures).*

We thank the reviewer for this helpful suggestion. We have now updated all relevant bar graphs to include individual data points for each biological replicate.

> *(9) The authors should validate the relative levels of a few DEGs shown in Figure 3F, Figure 3G, and Figure S4C, in the lung tissues of mice infected with wild-type, mutant, and complemented strains.*

We thank the reviewer for this suggestion. In the revised manuscript, we have performed qRT-PCR to validate the expression levels of selected DEGs, including inflammation-related and lysosome-associated genes, in lung tissues from mice infected with wild-type, mutant, and complemented strains (New Figure S8C-H).

> *(10) Did the authors perform an animal experiment using a mutant strain complemented with the phosphatase-deficient MmpE (Comp-MmpE-H348AN359H)?*

We appreciate the reviewer's comment. We agree that an additional animal experiment would be useful to assess the effects of the phosphatase. However, our study mainly focused on interpreting the function of the nuclear localization of MmpE during BCG infection. Additionally, we have assessed the role of the phosphatase of MmpE during infection with cell model (Figure 3E).

> *Minor comment:*
>
> *The mutant strain should be verified by either Southern blot or whole genome sequencing.*

We thank the reviewer for this comment. We verified deletion of *mmpE* gene by PCR method (Figure S3A-D) which was acceptable in many publications (Zhang et al., PLoS Pathog, 2020; Zhang et al., Nat Commun, 2022).

> ***Reviewer #3 (Recommendations for the authors):***
>
> *(1) Line 195: cytokine.*

We thank the reviewer for the comments. We have now corrected it.

> *(2) Line 225: rewording required.*

Corrected.

> *(3) Figure 4A. "No difference" instead of "No different".*

Corrected.

> *(4) "KommpE" should be replaced with "ΔmmpE strain" (Δ=delta symbol).*

Corrected.

> *(5) Supplementary Figure 7. The figure legend states CFU assays, but the y-axis and the graph seem to depict IS1081 quantification.*

We thank the reviewer for the comment. The figure is based on IS1081 quantification using qRT-PCR, not CFU assays. We have now revised the legend for New Figure S8A.

References

Chandra P, Ghanwat S, Matta SK, Yadav SS, Mehta M, Siddiqui Z, Singh A, Kumar D (2015) Mycobacterium tuberculosis Inhibits RAB7 Recruitment to Selectively Modulate Autophagy Flux in Macrophages Sci Rep 5:16320.

Darrah PA, Zeppa JJ, Maiello P, Hackney JA, Wadsworth MH 2nd, Hughes TK, Pokkali S, Swanson PA 2nd, Grant NL, Rodgers MA, Kamath M, Causgrove CM, Laddy DJ, Bonavia A, Casimiro D, Lin PL, Klein E, White AG, Scanga CA, Shalek AK, Roederer M, Flynn JL, Seder RA (2020) Prevention of tuberculosis in macaques after intravenous BCG immunization Nature 577:95-102.

Forrellad MA, Blanco FC, Marrero Diaz de Villegas R, Vázquez CL, Yaneff A, García EA, Gutierrez MG, Durán R, Villarino A, Bigi F (2020) Rv2577 of Mycobacterium tuberculosis Is a virulence factor with dual phosphatase and phosphodiesterase functions Front Microbiol 11:570794.

Innokentev A, Sanchez AM, Monetti M, Schwer B, Shuman S (2025) Efn1 and Efn2 are extracellular 5'-nucleotidases induced during the fission yeast response to phosphate starvation mBio 16: e0299224.

Keppetipola N, Shuman S (2008) A phosphate-binding histidine of binuclear metallophosphodiesterase enzymes is a determinant of 2',3'-cyclic nucleotide phosphodiesterase activity J Biol Chem 283:30942-9.

Lampe GD, King RT, Halpin-Healy TS, Klompe SE, Hogan MI, Vo PLH, Tang S, Chavez A, Sternberg SH (2024) Targeted DNA integration in human cells without double-strand breaks using CRISPR-associated transposases Nat Biotechnol 42:87-98.

Li Z, Sheerin DJ, von Roepenack-Lahaye E, Stahl M, Hiltbrunner A (2022) The phytochrome interacting proteins ERF55 and ERF58 repress light-induced seed germination in Arabidopsis thaliana Nat Commun 13:1656.

Marasco LE, Dujardin G, Sousa-Luís R, Liu YH, Stigliano JN, Nomakuchi T, Proudfoot NJ, Krainer AR, Kornblihtt AR (2022) Counteracting chromatin effects of a splicing-correcting antisense oligonucleotide improves its therapeutic efficacy in spinal muscular atrophy Cell 185:2057-2070.e15.

Martins WK, Santos NF, Rocha CS, Bacellar IOL, Tsubone TM, Viotto AC, Matsukuma AY, Abrantes ABP, Siani P, Dias LG, Baptista MS (2019) Parallel damage in mitochondria and lysosomes is an efficient way to photoinduce cell death Autophagy 15:259-279.

Master SS, Rampini SK, Davis AS, Keller C, Ehlers S, Springer B, Timmins GS, Sander P, Deretic V (2008) Mycobacterium tuberculosis prevents inflammasome activation Cell Host Microbe 3:224-32.

Matange N, Podobnik M, Visweswariah SS (2015) Metallophosphoesterases: structural fidelity with functional promiscuity Biochem J 467:201-16.

Niroula N, Ghodasara P, Marreros N, Fuller B, Sanderson H, Zriba S, Walker S, Shury TK, Chen JM (2025) Orally administered live BCG and heat-inactivated Mycobacterium bovis protect bison against experimental bovine tuberculosis Sci Rep 15:3764.

Palmieri M, Pal R, Nelvagal HR, Lotfi P, Stinnett GR, Seymour ML, Chaudhury A, Bajaj L, Bondar VV, Bremner L, Saleem U, Tse DY, Sanagasetti D, Wu SM, Neilson JR, Pereira FA, Pautler RG, Rodney GG, Cooper JD, Sardiello M (2017) mTORC1-independent TFEB activation via Akt inhibition promotes cellular clearance in neurodegenerative storage diseases Nat Commun 8:14338.

Péan CB, Schiebler M, Tan SW, Sharrock JA, Kierdorf K, Brown KP, Maserumule MC, Menezes S, Pilátová M, Bronda K, Guermonprez P, Stramer BM, Andres Floto R, Dionne MS (2017) Regulation of phagocyte triglyceride by a STAT-ATG2 pathway controls mycobacterial infection Nat Commun 8:14642.

Qu Z, Zhou J, Zhou Y, Xie Y, Jiang Y, Wu J, Luo Z, Liu G, Yin L, Zhang XL (2020) Mycobacterial EST12 activates a RACK1-NLRP3-gasdermin D pyroptosis-IL-1β immune pathway Sci Adv 6: eaba4733.

Shenoy AR, Capuder M, Draskovic P, Lamba D, Visweswariah SS, Podobnik M (2007) Structural and biochemical analysis of the Rv0805 cyclic nucleotide phosphodiesterase from Mycobacterium tuberculosis J Mol Biol 365:211-25.

Smith AA, Su H, Wallach J, Liu Y, Maiello P, Borish HJ, Winchell C, Simonson AW, Lin PL, Rodgers M, Fillmore D, Sakal J, Lin K, Vinette V, Schnappinger D, Ehrt S, Flynn JL (2025) A BCG kill switch strain protects against Mycobacterium tuberculosis in mice and non-human primates with improved safety and immunogenicity Nat Microbiol 10:468-481.

Wang J, Ge P, Qiang L, Tian F, Zhao D, Chai Q, Zhu M, Zhou R, Meng G, Iwakura Y, Gao GF, Liu CH (2017) The mycobacterial phosphatase PtpA regulates the expression of host genes and promotes cell proliferation Nat Commun 8:244.

Wang J, Li BX, Ge PP, Li J, Wang Q, Gao GF, Qiu XB, Liu CH (2015) Mycobacterium tuberculosis suppresses innate immunity by coopting the host ubiquitin system Nat Immunol 16:237–245

Wen X, Wang J, Zhang D, Ding Y, Ji X, Tan Z, Wang Y (2020) Reverse Chromatin Immunoprecipitation (R-ChIP) enables investigation of the upstream regulators of plant genes Commun Biol 3:770.

Xu X, Lu X, Dong X, Luo Y, Wang Q, Liu X, Fu J, Zhang Y, Zhu B, Ma X (2017) Effects of hMASP-2 on the formation of BCG infection-induced granuloma in the lungs of BALB/c mice Sci Rep 7:2300.

Zhang L, Hendrickson RC, Meikle V, Lefkowitz EJ, Ioerger TR, Niederweis M. (2020) Comprehensive analysis of iron utilization by Mycobacterium tuberculosis PLoS Pathog 16: e1008337.

Zhang L, Kent JE, Whitaker M, Young DC, Herrmann D, Aleshin AE, Ko YH, Cingolani G, Saad JS, Moody DB, Marassi FM, Ehrt S, Niederweis M (2022) A periplasmic cinched protein is required for siderophore secretion and virulence of Mycobacterium tuberculosis Nat Commun 13:2255.

Zhang X, He X, Li Q, Kong X, Ou Z, Zhang L, Gong Z, Long D, Li J, Zhang M, Ji W, Zhang W, Xu L, Xuan A (2017) PI3K/AKT/mTOR Signaling Mediates Valproic Acid-Induced Neuronal

Differentiation of Neural Stem Cells through Epigenetic Modifications Stem Cell Reports 8:1256-1269.

https://doi.org/10.7554/eLife.108037.2.sa0